4 Evaluation of Causes and Mechanisms of Irradiation-Assisted Cracking of Austenitic Stainless Steel in PWRs

4.1 Introduction

Field failures have been reported in various PWR core internal components fabricated from austenitic SSs, such as baffle bolts, control rod cladding, pins, keys, and bolts. Many of the failed components were fabricated from cold-worked materials of Types 316, 347, and 304 SS. Typically, failures of PWR core internals are intergranular (IG) and are observed at neutron-damage levels approximately a few orders of magnitude higher (i.e., >10 dpa) than the threshold damage level of BWR core internals (i.e., ≈0.7 dpa). At this time, the database and mechanistic understanding of PWR core internals are very limited, and it is not clear if the failures should be classified as IASCC or irradiation-assisted cracking (IAC).

The objectives in this task are to evaluate the susceptibility of austenitic SS core internals to IAC in PWRs as a function of the fluence, water chemistry, material chemistry, and cold-work. The program will focus on: (a) evaluation of the effects of PWR-like high fluence on susceptibility to IASCC, (b) neutron irradiation embrittlement, e.g., loss of fracture toughness, (c) void swelling behavior in austenitic SSs, (d) effect of cold-work and solution anneal, (e) fracture toughness and SCC behavior of cast duplex SSs at high fluence, and (f) effectiveness of mitigative measures, such as optimization of ferrite content, grain-boundary engineering, and minimization of S concentration. Tests will be conducted on material procured from EBR–II reactor fuel cans and on SS specimens irradiated in the BOR–60 reactor in Russia.

4.2 Irradiation of Austenitic Stainless Steels in the BOR-60 Reactor (H. M. Chung and W. K. Soppet)

An experiment has been initiated to irradiate specimens of various types of materials and geometry under PWR-like conditions. The irradiation experiment is being conducted jointly in cooperation with the Cooperative Irradiation-Assisted Stress Corrosion Cracking Research (CIR) Program. Irradiation of the specimens is performed in the BOR-60 Reactor, a sodium-cooled breeder reactor located in the Research Institute of Atomic Reactors (RIAR), Dimitrovgrad, Ulyansk Region, Russian Federation.

In the first part of the irradiation campaign, specimens were irradiated to ≈5 and ≈10 dpa in Irradiation Cycle BORIS-6 in flowing sodium maintained at 322.1-322.6°C. Further irradiation of specimens to ≈40 dpa in Irradiation Cycle BORIS-7 continues in the second part of the campaign.

After irradiation in BORIS-6, 48 tensile-specimens (contained in 12 bundles) and 166 disk-specimens (contained in 4 capsules) were discharged. Each bundle contains 4 tensile specimens and the disk capsules contain 23-56 disk specimens; see Figs. 25 and 26, respectively. The actual doses of the tensile-specimen bundles and disk-capsules are summarized in Table 14. HE10 is a sealed helium-tight capsule and AN40, AN20, AN10, and AN05 are “weeper” capsules perforated to allow circulation of sodium. Capsule AN-20, containing 53 disk specimens, accumulated 24.5 dpa. Twenty-three disk specimens contained in the helium-filled Capsule HE10 accumulated 11.8 dpa.

Table 14. Accumulated dose of 12 bundles containing tensile specimens and 4 capsules containing disk specimens discharged from BOR-60 reactor after irradiation at 322°C.

ID No. of Bundle (Each Contains 4 Tensile Specimens)	ID No. of Capsule Containing Disk-Specimens	Date Discharged from BOR-60	Actual Dose (dpa)
5-1		Oct., '01	5.5
5-2		Oct., '01	5.5
5-3		Oct., '01	5.5
5-4		Oct., '02	4.8
5-5		Oct., '02	4.8
5-6		Oct., '02	4.8
10-1		Oct., '01	10.2
10-3		Oct., '01	10.2
10-2		Oct., '01	11.8
10-4		Oct., '01	11.8
10-5		June, '01	10.4
10-6		June, '01	10.4
	AN 05 (56 disks)	Oct., '01	5.5
	AN 10 (34 disks)	Oct., '02	10.2
	HE 10 (23 disks)	Oct., '02	11.8
	AN 20 (53 disks)	March, '03	24.5

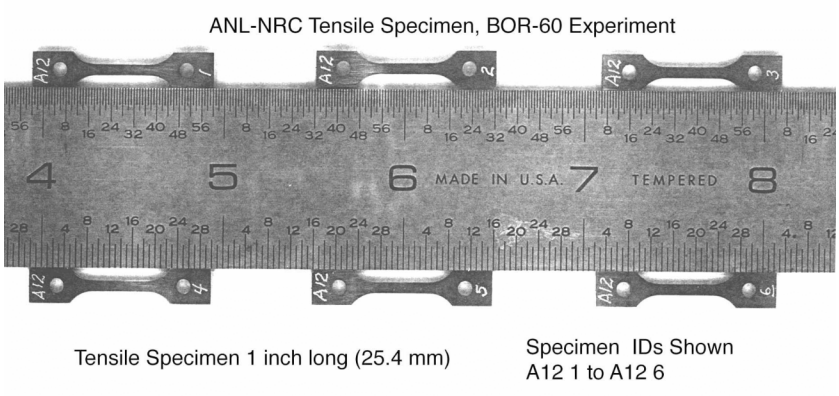

Figure 25. Tensile specimens irradiated in the BOR-60 reactor

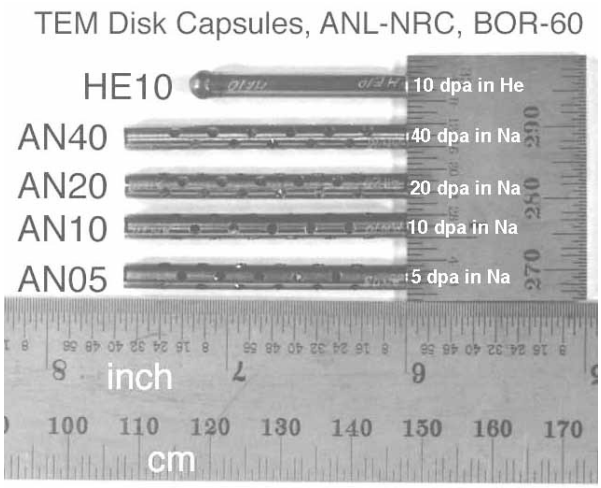

Figure 26. Disk-specimen capsules irradiated in the BOR-60 reactor. Note He-tight Capsule HE10 is sealed and "weeper" Capsules AN40, AN20, AN10, and AN05 are perforated to allow circulation of sodium.

Eight more bundles containing 32 tensile specimens are still being irradiated. A total of 24 specimens irradiated ≈5 dpa and 56 specimens irradiated to ≈10 dpa are expected to be available for testing tensile and stress-corrosion-cracking behavior of various steels. Table 15 gives a summary of breakdown of the number of specimen, steel type, and material state for damage levels of ≈5 and ≈10 dpa.

Table 15. Summary of number, steel type, and material state of tensile specimens irradiated to ≈5 or ≈10 dpa in BOR-60 reactor.

	Material Type[a]	Description of Material[a]	Heat ID	Material Code[b]	SSRT 5 dpa	SSRT 10 dpa
1	347 SA	commercial 347 SS, solution-annealed	316642	D1	1	2
2	347 CW	commercial heat 347, cold-worked	316642CW	D2	2	2
3	316 SA	316, Heat B, solution-annealed	2333	B1		2
4	316 CW	316, Heat B, cold-worked	2333 CW	B2		2
5	316LN SA	316LN, solution-annealed	623	B3	1	2
6	316LN-Ti SA	316LN, Ti-doped, solution-annealed	625	B4	1	2
7	316 SA	316, solution-annealed	C21	B5	1	3
8	316 CW	316, cold-worked	C21 CW	B6	2	3
9	316 WW	316, warm-worked	C21 WW	B7		2
10	CF-3 cast	cast keel block, ferrite content 13.5%	52	C1		2
11	CF-8 cast	cast keel block, ferrite content 13.5%	59	C2		2
12	CF-3 cast	cast steel, ferrite content 23%	69	C3		
13	CF-8 cast	cast steel, ferrite content 23%	68	C4		
14	304 SA	commercial heat 304, SA, low S	C1	A1	1	2
15	304 SA	commercial heat 304, SA, high S	C9	A2	1	2
16	304 SA	commercial heat 304, SA, low S	C12	A3	1	2
17	304 CW	commercial heat 304, cold-worked	C1 CW	A4	1	2
18	304 CW	commercial heat 304, cold-worked	C12 CW	A5	1	2
19	304 GBE	grain-boundary-optimized 304 SS	304 GBE	A6	1	2
20	316 GBE	grain-boundary-optimized 316 SS	316 GBE	B8	1	2
21	690 GBE	grain-boundary-optimized Alloy 690	690 GBE	E1	1	2
22	304 BASE	304 SS, base heat of 304 GBE	304 BASE	A7	1	2
23	316 BASE	316 SS, base heat of 316 GBE	316 BASE	B9	1	2
24	690 BASE	Alloy 690, base heat of 690 GBE	690 BASE	E2	1	2
25	HP 304L SA	HP 304L, high O, solution-annealed	945	A8	1	2
26	HP 304L SA	HP 304L, low O, solution-annealed	1327	A9	1	2
27	304L SA	commercial heat 304L, SA	C3	A10	1	2
28	304L CW	commercial heat 304L, cold-worked	C3 CW	A11	1	2
29	304-like alloy	lab alloy, 21wt.% Cr, ≈2% ferrite, SA	L5	A12	1	2
Total					24	56

[a]SA = solution-annealed; CW = cold-worked at room temperature; WW = warm-worked at 400°C; GBE = grain-boundary-engineered; BASE = base heat for GBE modification; HP = high-purity.
[b]A = Type 304, B = Type 316, C = cast, and D = Type 347 stainless steels; E = Alloy 690.

4.3 Studies on Intergranular-Fracture Characteristics

Selected specimens irradiated in the Halden reactor or in commercial BWRs were fractured in inert environments after SSRT testing in water or after charging with hydrogen. The objective of this study was to perform low-cost fracture tests that could provide insights helpful to understand the mechanism of PWR IASCC.

4.3.1 Intergranular Fracture in Inert Environment

Needle-like specimens were prepared from selected BWR neutron absorber tubes and a control blade sheath. After cathodically charging with hydrogen at ≈50°C in a solution that contains 100-mg/L

$NaAsO_2$ dissolved in 0.1-N H_2SO_4 (current density during H charging ≈500 mA/cm^2), the needle-like specimens were fractured at 23°C in the vacuum environment of an Auger electron microscope (AEM). The procedures of the bend fracture at 23°C in air or in vacuum (H-charged needles) are illustrated in Fig. 7. Chemical composition, fluence, and the results of fractography of the BWR components are given in Table 16. The table also summarizes the results of SSRT tests for the same BWR components (in 289°C water, DO ≈0.3 ppm) conducted and reported previously.[82]

Table 16. Tests on BWR components; SSRT test in 289°C water (0.3 ppm DO) and bend fracture in 23°C vacuum after H-charging.

Heat ID No.[a]	Cr	Ni	Mn	C	N	Si	P	S	Fluence (10^{21} n/cm^{-2})	%IGSCC, from SSRT in 289°C water, DO ≈0.3 ppm	Depth of IG fracture in vacuum after H-charging (μm)
HP304-B	18.50	9.45	1.53	0.018	0.100	<0.03	0.005	0.003	1.4	58	1, 26
HP304-CD	18.58	9.44	1.22	0.017	0.037	0.02	0.002	0.003	1.4	32	37, 58
CP304-A	16.80	8.77	1.65	–	0.052	1.55	–	–	2.0	28	37, 45
CP304-B	–	–	–	–	–	–	–	–	2.4	3, 5	58, 72

[a]HP304-B and –CD are high-purity Type 304L SS BWR neutron absorber tubes.
CP304-A is a commercial-purity 304 SS BWR neutron absorber tube.
CP304-B is a commercial-purity 304 SS BWR control blade sheath.

For steels irradiated in the Halden Reactor and tested in 289°C water (SSRT test, DO ≈8 ppm; see Table 8), it was noticed that susceptibilities to IG failure in water and in 23°C air (bend fracture) are inverted. That is, steels that showed high susceptibility to IASCC in 289°C water (e.g., C9-03, C19-03, and L18-03) exhibited low susceptibility to intergranular cracking (IGC) in 23°C air, whereas steels that showed low susceptibility to IASCC in 289°C water (e.g., C12-03, C10-03, and C1-03) exhibited high susceptibility to IGC in 23°C air. This trend is shown graphically in Fig. 27 top.

A similar trend was observed for BWR components, see Fig. 27 bottom and Table 16. That is, BWR components that showed high susceptibility to IASCC in 289°C water exhibited low susceptibility to IGC in 23°C vacuum when fractured after H-charging, whereas components that showed low susceptibility to IASCC in 289°C water exhibited high susceptibility to IGC in 23°C vacuum.

In the fracture of H-charged BWR components in 23°C vacuum, H charging was the direct cause that rendered the materials susceptible to IG fracture. When a specimen from the BWR components was not charged with H (i.e., material in as–irradiated state), no IG fracture could be induced in the 23°C vacuum. Based on this observation and considering essentially the same trend in Fig. 14, we conclude that the major process leading to IG fracture in air (in the Halden-Reactor-irradiated specimens, Fig. 27 top) and in vacuum (in the H-charged BWR components, Fig. 27 bottom) was the same, i.e., H-induced IG fracture.

The observation that steels containing a very low or negligible amount of S are immune or virtually immune to IASCC may provide an important clue to understanding the behavior manifested in Fig. 27 and help to understand IGC behavior in inert environments or low-ECP water.

Heuer and coworkers investigated the effect of ion-implanted S on disorder-induced amorphization of Ni.[108] They also investigated the effects of thermal segregation of S on GBs on the mechanical properties of unirradiated binary Ni–S. In the latter investigation, they found that as GB concentration of S exceeds ≈10 at.% (≈5.6 wt.%), the mechanical properties of S–segregated Ni start to degrade drastically in 23°C air, i.e., drastic decrease in total elongation, tensile strength, modulus of toughness, reduction-in-area, and drastic increase in percent IGC. Okamoto and coworkers also showed that the volume fraction

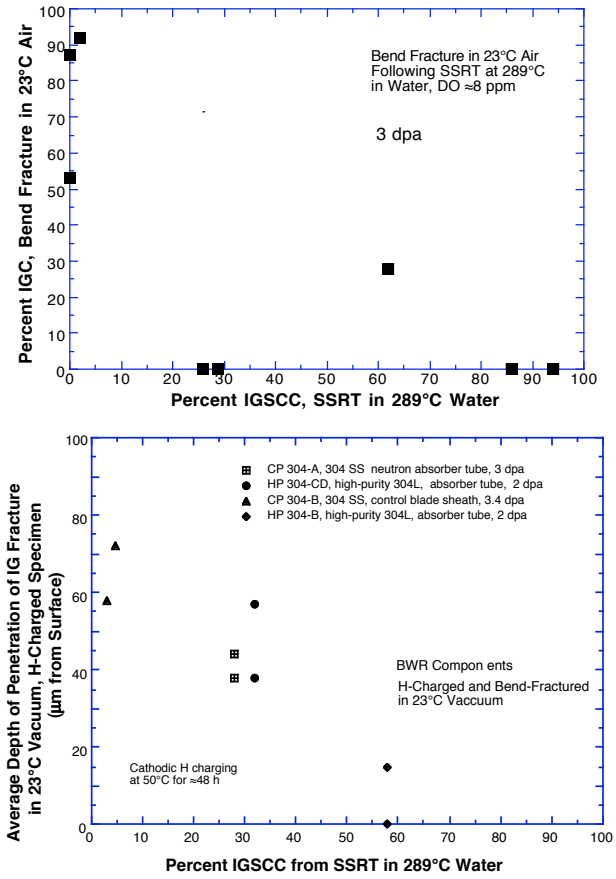

Figure 27. Susceptibility to IG fracture in 289°C water and in inert environment at 23°C. Top: %IGSCC from SSRT in 289°C water (DO ≈8 ppm) vs. %IGC from bend fracture in 23°C air (steels irradiated in the Halden Reactor). Bottom: %IGSCC from SSRT in 289°C water (DO ≈0.3 ppm) vs. %IGC from bend fracture in 23°C vacuum (H-charged BWR components).

of amorphization of the S–ion-implanted specimens starts to increase drastically when the bulk S concentration exceeds ≈10 at.%.[109] Based on these observations, they concluded that S–induced IG fracture in binary Ni–S is explained well by disorder-induced melting of a Ni– and S–rich thin film on GBs.[108,109] They also proposed that this process is strongly influenced by S concentration, H concentration, stress, temperature, and irradiation damage.

We believe that the model of Okamoto and his coworkers, advanced to explain IG fracture of bulk unirradiated Ni–S–H, is a very useful starting point in an attempt to better understand our observations. We propose a modification of the model to reflect the consideration that the H concentration in S–rich GB thin film should decrease strongly as temperature increases. This is because the diffusivity of H in Ni increases strongly as temperature increases. As a result, it becomes increasingly difficult to prevent diffusion of H atoms into the grain matrix, and hence, to maintain critical hydrogen concentration in the thin film near the GB. This situation is shown schematically in Fig. 28. The figure predicts that the effect of H on IG fracture would be significant at low temperatures (e.g., H-induced IG fracture at 23°C in the steels shown in Fig. 27), but that the effect of H becomes increasingly insignificant at higher temperatures.

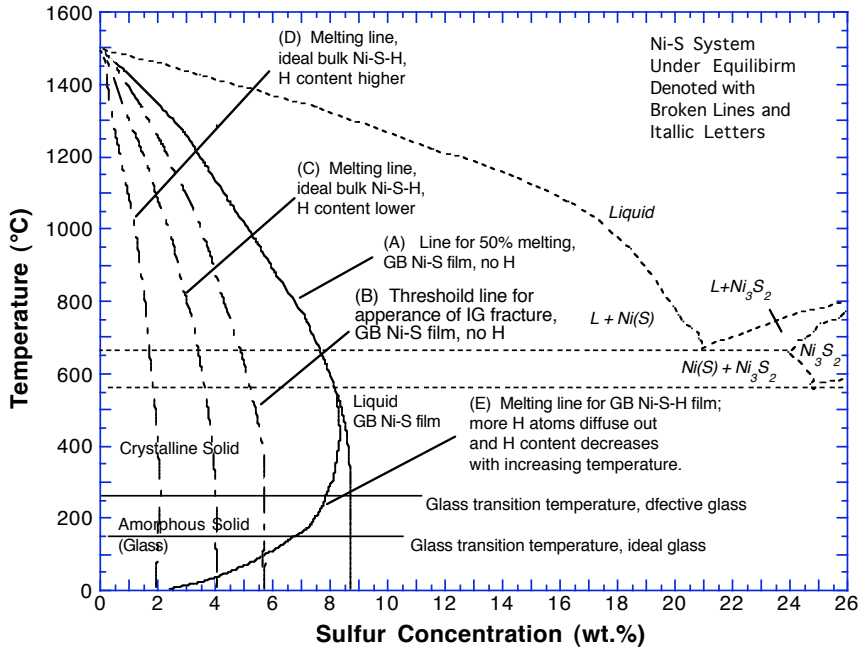

Figure 28. Schematic illustration of various threshold boundaries applicable to disorder-induced melting or amorphization of Ni–S–H grain-boundary thin film.

4.3.2 Initial Model of IASCC

In view of several key observations reported in this study and elsewhere, an inital IASCC mechanism for irradiated austenitic SS is being considered. The model, schematically illustrated in Fig. 29, takes into account four key observations:

(a) Dominant effect of S (this study, Figs 9–11).

(b) Evidence of GB segregation of S in unirradiated steel (Ref. 86) and in irradiated BWR components (this study Fig. 15).

(c) Properties of binary Ni–S that contain Ni– and S–rich thin film on grain boundaries (GBs) (Refs. 108 and 109).

(d) Crack-tip microstructure and microchemistry of unirradiated and irradiated steels, reported by, respectively, Dumbill[110] and Thomas and Bruemmer.[111]

Furthermore, to better understand the IASCC mechanism, it is important to consider the following:

(a) Strong dependence of IASCC susceptibility on fluence.

(b) Strong dependence of IASCC susceptibility on S concentration at high fluence.

(c) Strong dependence of S effect on fluence for S > 0.003 wt.%.

(d) Indication that the deleterious effect of S saturates at concentrations higher than ≈0.006 wt.% S.

(e) At very low concentrations of S (e.g., ≤0.002 wt.%) Type 304 and 316 steels containing ≥0.03 wt.% C are virtually immune to IASCC.

(f) The trend that a high concentration of C reduces the deleterious effect of S at low S concentrations.

(g) Very low solubility of S in austenitic SS at ≈300°C. In as–fabricated state, the distribution of S atoms (i.e., in solution in grain matrices, on GBs, or in Mn sulfides) is influenced strongly by Mn content and fabrication history (i.e., ingot melting, cooling, intermediate anneal, and final anneal).

(h) Thermal segregation of S to GBs during fabrication.

(i) Possible irradiation-induced GB segregation of S.

(j) Parallel GB Cr depletion and GB Ni segregation.

(k) Strong influence of DO and electrochemical potential on IASCC susceptibility.

(l) Strong effect of strain rate on percent IGSCC from SSRT tests.

The model depicted in Fig. 29 is based on the following steps, some postulated and some supported by observations in this study or other investigations described below:

(a) When a crack tip encounters a GB, the metal in front of the crack tip is oxidized preferentially along the GB, because stress and defects are higher at the GB. The GB is a preferential path for faster diffusion of O and H from the water.

(b) The metal at the front of the crack tip is gradually converted to Fe-Cr spinel oxide, because Fe and Cr are readily oxidized in high-temperature water.

(c) Nickel atoms are more difficult to oxidize than Fe and Cr. The free energies of oxidation at ≈300°C of Ni, Fe, and Cr are, respectively, –92, –111, and –155 kcal/mole O_2. Thus, most Ni atoms are least readily oxidized. As a result, Ni atoms are gradually pushed out of the growing GB Fe-Cr spinel oxide.

(d) At the same time, S atoms are also pushed out of the spinel oxide, because the solubility limit of S is lower in spinel than in metal and the affinity of S to Ni is strong.

(e) Eventually, Ni– and S–rich thin films form at the boundary between the spinel oxide and metal matrix and at the tip of the growing oxide sheet. The Ni– and S–rich region can be in the shape of a continuous or discontinuous film or a small island.

(f) Some S ions accumulated in the crack tip water diffuse into the thin region of metal in contact with the Ni– and S–rich film under high tensile stress.

(g) When the S concentration in the Ni– and S–rich thin film or island exceeds a threshold level (see Fig. 28), it melts or is amorphized, thereby losing its metallic strength. When the Ni– and S–rich thin film or island melts, voids and cavities are formed, preferentially at the oxide tip and near the oxide/metal boundary.

(h) Then, the crack tip advances along the weakened metal/oxide boundary, i.e., along the molten or amorphized Ni–S thin film.

(i) Once the Ni– and S–rich thin films or islands melt or are amorphized, they lose the crystalline structure. The polyhedral crystal structure of the thin film, such as that described by Ashby and Spaegen,[112] is broken, and the S atoms incorporated in the polyhedral cages diffuse back into the metal matrix.

(j) Depending on the service history and post-failure thermal conditions, S–rich thin film or islands may or may not be present in local spots.

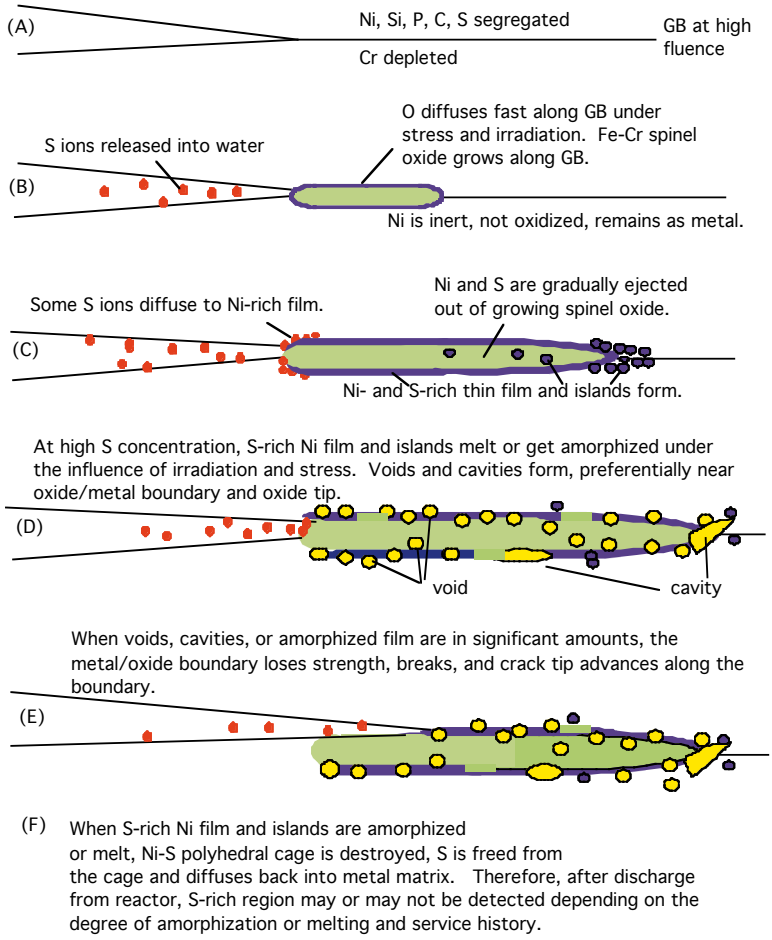

Figure 29. Schematic illustration of a proposed IASCC model

5 Cracking of Nickel Alloys and Welds (W. K. Soppet, O. K. Chopra, and W. J. Shack)

5.1 Introduction

This part of the study consists primarily of establishing CGRs under constant and cyclic loading and evaluating Ni alloys and weld metals metallographically to develop comprehensive and statistically significant analyses that could be used to determine the dependence of the SCC of these materials on alloy composition, microstructure, water chemistry, temperature, and other factors. High–Ni alloys have experienced general corrosion (tube wall thinning), localized intergranular attack (IGA), and SCC in LWRs. Secondary–side IGA* and axial and circumferential SCC** have occurred in Alloy 600 tubes at tube support plates in many steam generators. Primary–water SCC of Alloy 600 steam generator tubes in PWRs at roll transitions and U–bends and in tube plugs*** is a widespread problem that has been studied intensively. In the primary system of PWRs, cracking has occurred in Alloy 600 and other high–Ni alloys that are used in applications such as instrument nozzles and heater thermal sleeves in the pressurizer,† penetrations for the control–rod drive mechanism in the closure heads of reactor vessels,†† and in dissimilar–metal welds between SS piping and low–alloy steel nozzles.††† In BWRs, cracking has occurred in jet pump hold–down beams§ and in shroud–support–access–hole covers.§§ Alloy 690, with a higher Cr content and greater resistance to SCC, has been proposed as an alternate to Alloy 600.

A program is being conducted at ANL to evaluate the resistance of Alloys 600 and 690 and their welds to EAC in simulated LWR coolant environments. Fracture mechanics CGR tests have been conducted on CT specimens of Alloys 600 and 690 in either oxygenated high–purity water or deaerated water that contained B, Li, and low concentrations of dissolved H at 289–320°C. The results have been presented elsewhere.[113–120] Because environmental degradation of the alloys in many cases is very sensitive to processing, the effects of various thermomechanical treatments have also been evaluated.

To obtain a qualitative understanding of the degree and range of conditions that are necessary for significant environmental enhancement of growth rates in LWR environments, the experimental CGRs have been compared with CGRs that would be expected in air under the same mechanical loading conditions. In air, fatigue CGRs are generally represented by the equation

$$da/dN = C(T)\, F(f)\, S(R)\, (\Delta K)^n, \tag{25}$$

*NRC Information Notice No. 1991–67, "Problems with the Reliable Detection of Intergranular Attack (IGA) of Steam Generator Tubing," Oct. 1991.

**NRC Information Notice No. 1990–49, "Stress Corrosion Cracking in PWR Steam Generator Tubes," Aug. 1990; Notice No. 1996–38, "Results of Steam Generator Tube Examinations," June 1996; Notice No. 2001–16, "Recent Foreign and Domestic Experience with Degradation of Steam Generator Tubes and Internals," Oct. 2001.

***NRC Regulatory Issue Summary 2000–022, "Issues Stemming from NRC Staff Review of Recent Difficulties Experienced in Maintaining Steam Generator Tube Integrity," Nov. 2000; Information Notice No. 1997–26, "Degradation in Small-Radius U-bend Regions of Steam Generator Tubes," May 1997; Notice No. 1994–87, "Unanticipated Crack in a Particular Heat of Alloy 600 Used for Westinghouse Mechanical Plugs for Steam Generator Tubes," Dec. 1994.

†NRC Information Notice No. 1990–10, "Primary Water Stress Corrosion Cracking (PWSCC) of Inconel 600," Feb. 1990.

††NRC Generic Letter 1997-01: "Degradation of Control Rod Drive Mechanism and Other Vessel Closure Head Penetrations," Apr. 1, 1997; USNRC Bulletin 2001–01, "Circumferential Cracking of Reactor Pressure Vessel Head Penetration Nozzles," Aug. 2001; Bulletin 2002–01, "Reactor Pressure Vessel Head Degradation and Reactor Coolant Pressure Boundary Integrity," March 2002.

†††NRC Information Notice 2000–17, "Crack in Weld Area of Reactor Coolant System Hot Leg Piping at V. C. Summer," Oct. 2000; Supp. 1, Nov. 2000; Supp. 2, Feb. 2001.

§NRC Information Notice 1993–101, "Jet Pump Hold–Down Beam Failure," Dec. 1993.

§§NRC Information Notice 1992–57, "Radial Cracking of Shroud Support Access Hole Cover Welds," Aug. 1992.

where the functions C, F, and S express the dependence of temperature, frequency, and stress ratio, and n is the exponent for the power–law dependence of growth rates on the stress intensity factor range ΔK. The effect of temperature, stress ratio R, cyclic frequency, and stress intensity factor range ΔK on the CGRs was established from an analysis of the existing fatigue CGR data.[117] The CGR (m/cycle) of Alloy 600 in air is expressed as

$$da/dN = C_{A600} (1 - 0.82\ R)^{-2.2} (\Delta K)^{4.1}, \quad (26)$$

where ΔK is in MPa·m$^{1/2}$, and the constant C_{A600} is given by a third-order polynomial of temperature T (°C) expressed as

$$C_{A600} = 4.835 \times 10^{-14} + (1.622 \times 10^{-16})T - (1.490 \times 10^{-18})T^2 + (4.355 \times 10^{-21})T^3. \quad (27)$$

The fatigue CGRs of Alloy 600 are enhanced in high–DO water. The environmental enhancement of growth rates does not appear to depend on either the C content or heat treatment of the material. The CGRs at 320°C are comparable to those at 289°C. In contrast to the behavior in high–DO water, environmental enhancement of CGRs of Alloy 600 in low–DO water seems to depend on material conditions such as yield strength and grain boundary coverage of carbides. Materials with high yield strength and/or low grain boundary coverage of carbides exhibit enhanced CGRs. Correlations have been developed for estimating the enhancement of CGRs of Alloy 600 in LWR environments relative to the CGRs in air under the same loading conditions.

5.2 Experimental

The crack growth tests were conducted according to ASTM Designation E 647 "Standard Test Method for Measurement of Fatigue Crack Growth Rates." The tests were performed under controlled loading conditions with hydraulic closed–loop servo–controlled machines. The contribution to the load that arises from the pressure difference between the inside and the outside of the autoclave was taken into consideration. Crack length was monitored by DC potential–drop measurements. The redox and open–circuit corrosion potentials were monitored at the autoclave outlet by measuring the ECPs of platinum and an Alloy 600 electrode, respectively, against a 0.1–M KCl/AgCl/Ag external (cold) reference electrode. The effluent DO concentration and conductivity were also monitored during the tests. A detailed description of the test facility and test procedure is presented elsewhere.[119] The composition of Alloy 600 (Heat NX131031) used for the present CGR tests is given in Table 17.

Table 17. Composition (wt.%) of Alloy 600 Heat NX131031 base metal

Analyst	C	Mn	Fe	S	P	Si	Cu	Ni	Cr	Ti	Nb	Co
Vendor	0.07	0.22	7.39	0.002	0.006	0.12	0.05	76.00	15.55	0.24	0.07	0.058
ANL	0.07	0.22	7.73	0.001	–	0.18	0.06	75.34	–	–	–	–

The CGR tests were conducted in load–control mode using a sawtooth or trapezoidal waveform with load ratio R of 0.2–0.7. The specimen was precracked in the test environment at temperature, R = 0.2, and K_{max} of 20–24 MPa·m$^{1/2}$, to allow a crack advance of ≈2.5 mm. The corrosion fatigue tests were conducted at R = 0.7 and a sawtooth waveform with a 12–3000–s rise time and 1–s return time. The SCC growth rates were determined from constant load tests with periodic unloading to R = 0.7 every 3600 s; the time period for the unload/reload cycle was 4 s.

5.3 Results

The environmental and loading conditions, and the measured CGRs for specimen CT31–04 are given in Table 18. The change in crack length and K_{max} during the various test periods is shown in Fig. 30. The test was initiated at 289°C in high–purity water with ≈300 ppb DO. After ≈2700 h, the DO level was decreased to ≈5 ppb by periodic sparging the feedwater tank with nitrogen + 5% hydrogen and maintaining a 34–kPa overpressure of the gas mixture to provide ≈115 ppb dissolved hydrogen in water. The changes in crack length and ECP of Pt and SS electrodes during the transition period are shown in Fig. 31. The change in the SS ECP was slower than in the Pt ECP. For example, although the Pt ECP decreased to –400 mV (SHE) in 24 h, it took nearly 200 h for the steel to decrease to –300 mV (SHE). After the desired DO level was achieved, the system was operated for additional 200 h to allow the environmental conditions to stabilize. Also, the autoclave temperature was increased from 289 to 320°C. The DC potential system was reinitialized and the test restarted at $K_{max} \approx 36$ MPa $m^{1/2}$, R = 0.7, and 1000 s rise time, Fig. 30c. After ≈3700 h, the cover gas above the feedwater tank was changed to pure hydrogen gas maintained at 34–kPa overpressure to provide ≈2 ppm (≈23 cc/kg) dissolved hydrogen in water.

Table 18. Crack growth results for mill annealed Alloy 600[a] in high–purity water at 290 and 320°C

Test Period	Test Time, h	Temp., °C	O_2[b] Conc. ppb	ECP[b] mV (SHE) at 289°C SS	ECP[b] mV (SHE) at 289°C Pt	Load Ratio	Rise Time s	K_{max}[c], MPa·$m^{1/2}$	ΔK, MPa·$m^{1/2}$	Growth Rate, m/s	Crack Length, mm
Pre a	74	289	330	–	–	0.2	10	20.2	16.2	9.97E-10	12.80
Pre b	174	289	320	–	–	0.2	8	21.8	17.5	1.94E-09	13.48
Pre c	241	289	285	–	–	0.2	8	22.6	18.1	5.31E-09	14.19
Pre d	313	289	285	–	–	0.2	12	23.7	18.9	3.11E-09	15.04
Pre e	387	289	300	–	–	1.0	–	3.2	–		15.07
1	411	289	300	117	232	0.5	12	28.7	14.3	2.03E-09	15.25
	530	289	300	–	–	1.0	–	9.0	–		
2	823	289	303	–	–	0.7	300	28.6	8.6	2.7E-10	15.47
3	1154	289	298	114	230	0.7	1000	28.7	8.6	1.18E-10	15.63
4	1401	289	286	–	–	1.0	–	28.7	–	1.58E-11	15.68
5	1712	289	284	–	–	0.7	3000	28.8	8.6	7.87E-11	15.76
6	2021	289	282	102	222	1.0	–	29.1	–	4.42E-11	15.82
7a	2125	289	292	111	218	0.5	12	30.0	15.0	1.43E-09	16.41
7b	2186	289	292	–	–	0.5	12	30.6	15.3	1.79E-09	16.80
8	2242	289	287	–	–	0.7	12	30.9	9.3	9.31E-10	16.99
9	2450	289	276	–	–	1.0	–	35.0	–	4.37E-11	17.03
10	2496	289	370	–	–	0.7	12	35.4	10.6	2.18E-09	17.22
11	2706	289	375	119	219	0.7	1000	35.5	10.6	1.00E-10	17.29
12	3270	320	5[d]	–	–	0.7	1000	35.9	10.8	1.19E-10	17.48
13	3509	320	5[d]	-288	-473	1.0	–	36.0	–	5.78E-11	17.54
14	3739	320	5[e]	–	–	0.7	1000	36.3	10.9	2.00E-10[f]	17.73

[a]Compact tension specimen (1T CT) #CT31–04 of mill–annealed Alloy 600 (Heat NX131031).
[b]Effluent dissolved oxygen concentration and ECP. Effluent conductivity was 0.2–0.3 μS/cm. Feedwater conductivity at 25°C 0.06 μS/cm and pH at 25°C 6.6.
[c]Stress intensity, K_{max}, values at the end of the time period.
[d]Nitrogen + 5% hydrogen cover gas to provide 115 ppb dissolved hydrogen in water.
[e]Pure hydrogen cover gas to provide ≈2 ppm dissolved hydrogen in water.
[f]Estimated value, the DC potential drop system malfunctioned in the middle of the test period.

After the test, the specimen was fractured, and a detailed metallographic examination of the specimen was performed to validate the measurements of crack length by the DC potential method. A photograph of the broken top half of the specimen is shown in Fig. 32, a SEM photomicrograph of the

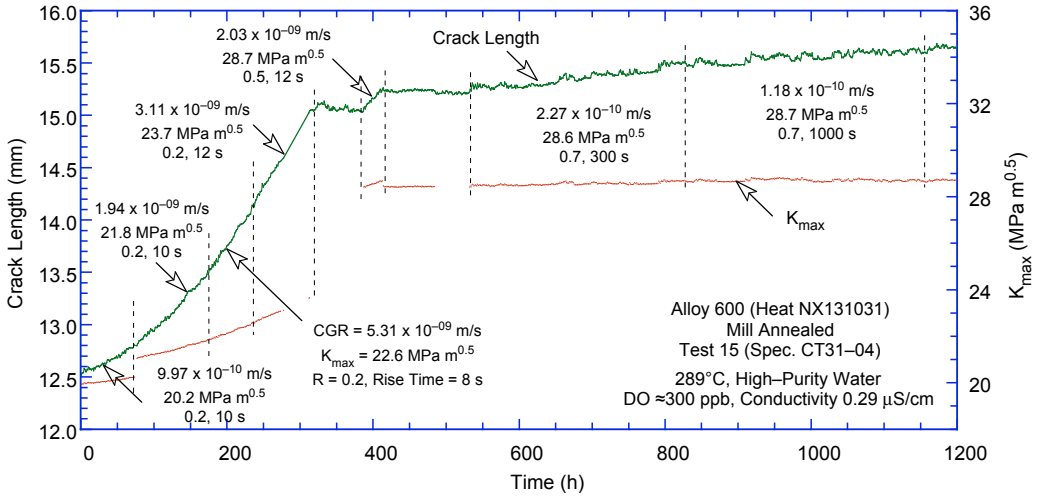

(a)

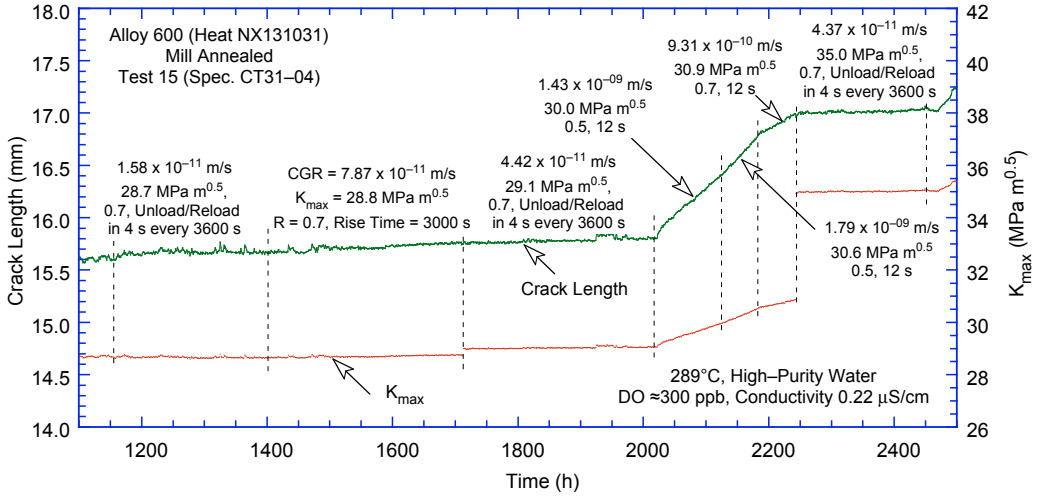

(b)

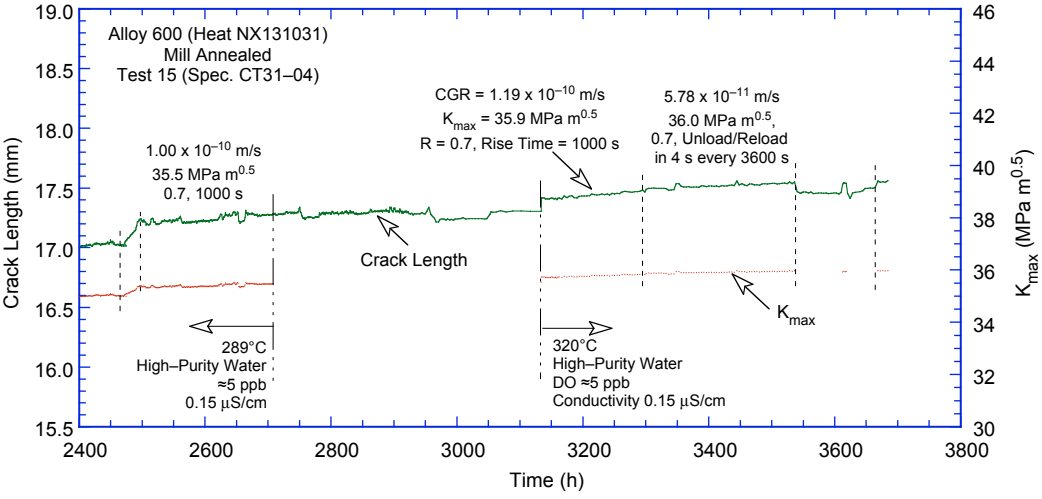

(c)

Figure 30. Crack–length–vs.–time plot for mill–annealed Alloy 600 specimen in high–purity water at 289 and 320°C: (a) 100–1200 h, (b) 1100–2500 h, and (c) 2400–3600 h.

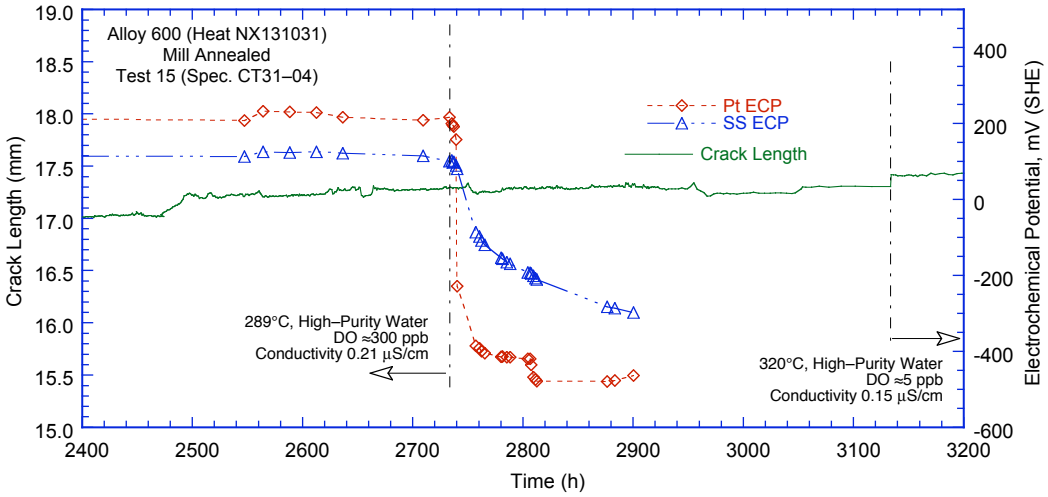

Figure 31. Change in crack length and ECP of Pt and stainless steel electrodes when the dissolved oxygen was decreased from ≈300 to 5 ppb.

surface after it was chemically cleaned is shown in Fig. 33. The fracture mode is primarily transgranular (TG) with two regions of intergranular (IG) fracture, first in high–DO water at 289°C and the second in low–DO water at 320°C. The final crack length and crack lengths at the start and end of first IG region (marked IG–1 in Fig. 33) were determined by the 9/8 averaging technique, i.e., the two–near–surface measurements were averaged and the resultant value was averaged with the remaining seven measurements. The measured value of the final crack length showed good agreement with the value estimated from the DC potential measurements.

Metallographic examination of the fracture surfaces indicates that the crack front was relatively straight during the various test periods. For example, in both high– and low–DO water the transition from TG to IG cracking occurred along a straight crack front. However, the IG region in high–DO water at 289°C is not uniform across the width of the specimen, it is wider in the middle than near the sides of the specimen, Figs. 32 and 33. In this region, IG cracking appears to have started during test period 4 and

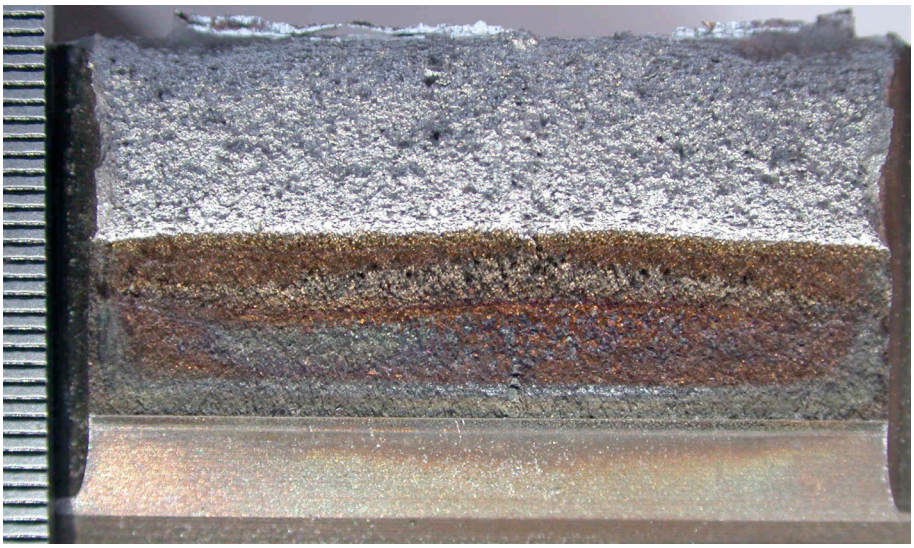

Figure 32. Photograph of the fracture surface of Alloy 600 specimen CT31–04.

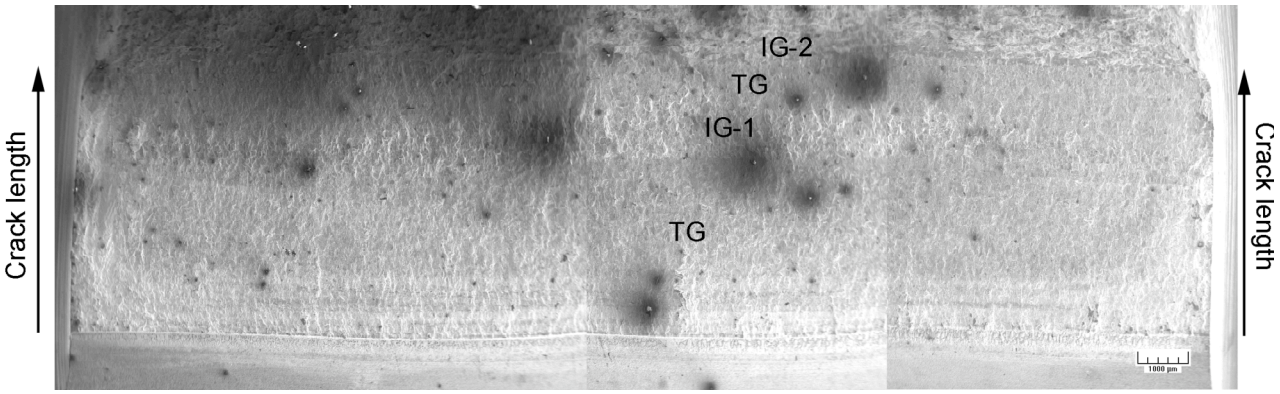

Figure 33. SEM photomicrograph of the fracture surface of Alloy 600 specimen CT31–04 after the surface oxide film was chemically removed.

continued through periods 5–7. Test periods 4–6 represent either constant load with periodic partial unloading every 3600 s or cyclic loading with 3000 s rise time. Test period 7 represents cyclic loading with 12 s rise time, the change in fracture mode from IG back to TG occurred during this test period. However, the change to TG cracking most likely occurred sooner near the sides than in the middle of the specimen resulting in a nonuniform crack front. The second IG region near the final crack front represents crack growth in low–DO water at 320°C during test periods 13 and 14.

A photomicograph of the entire crack extension in the middle of the specimen and higher magnification micrographs of the fracture morphology in different regions of the specimen are shown in Fig. 34. The TG fracture morphology consists of a faceted surface with occasional river patterns. The two regions of IG fracture show significant secondary IG cracks. However, there are some differences in the fracture morphology in regions IG–1 and IG–2, Fig. 35. Region IG–1 consists of predominantly IG facets with relatively smooth grain boundary surfaces, very few regions show TG facets. The fracture morphology in region IG–2 is a combination of IG and TG facets, the grain boundary surfaces are rough and the TG facets show occasional river patterns.

5.3.1 Fatigue Crack Growth Rates

The fatigue CGRs for Heat NX131031 in high–DO water at 289°C and low–DO water at 320°C are plotted in Fig. 36 as a function of the CGRs predicted in air for Alloy 600 under the same loading conditions. Results for the same heat of Alloy 600 in the MA and MA plus 30% CW conditions are also included in the figure. The CGRs (da/dN in m/cycle) in air were determined from Eqs. 26 and 27. In both high– and low–DO environments, the results for specimen CT31–04 of MA Heat NX 131031 show excellent agreement with those obtained earlier for specimen CT31–03 of the same material. In high–DO water at 289°C the CGRs for MA Heat NX131031 are slightly higher than the rates predicted by the best–fit curve proposed by Kassner and Shack[115] for Alloy 600 in high–purity water with ≈300 ppb DO, given by the expression

$$CGR_{env} = CGR_{air} + 4.4 \times 10^{-7} (CGR_{air})^{0.33}. \quad (28)$$

In low–DO water at 320°C the CGRs for MA Heat NX131031 follow the Kassner/Shack curve for high–DO water.

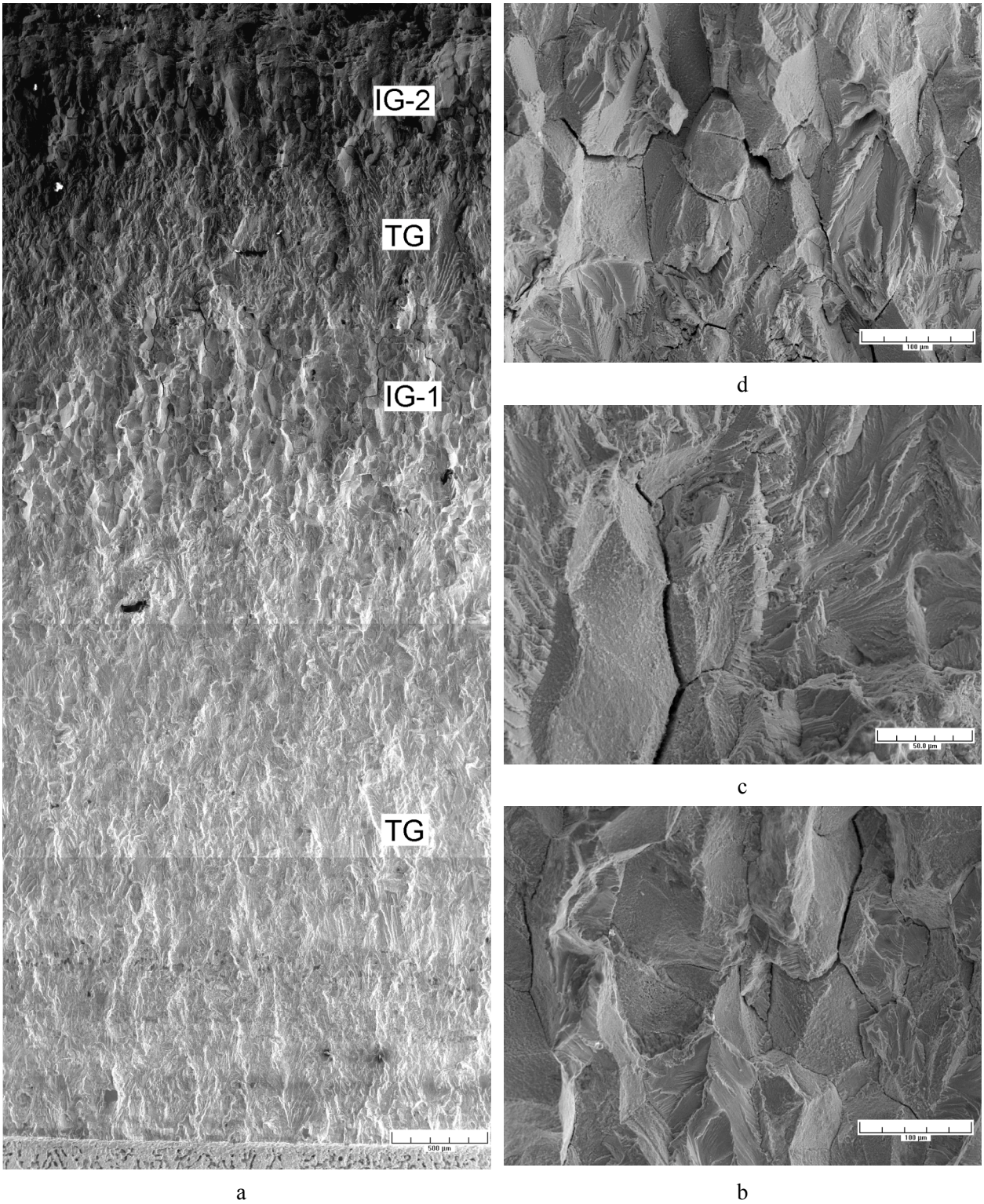

a b c d

Figure 34. (a) Photomicrograph of a region in the middle of the specimen showing the entire crack extension, (b) typical fracture surface in region IG–1, (c) transition from IG to TG, and (d) typical fracture surface in region IG–2.

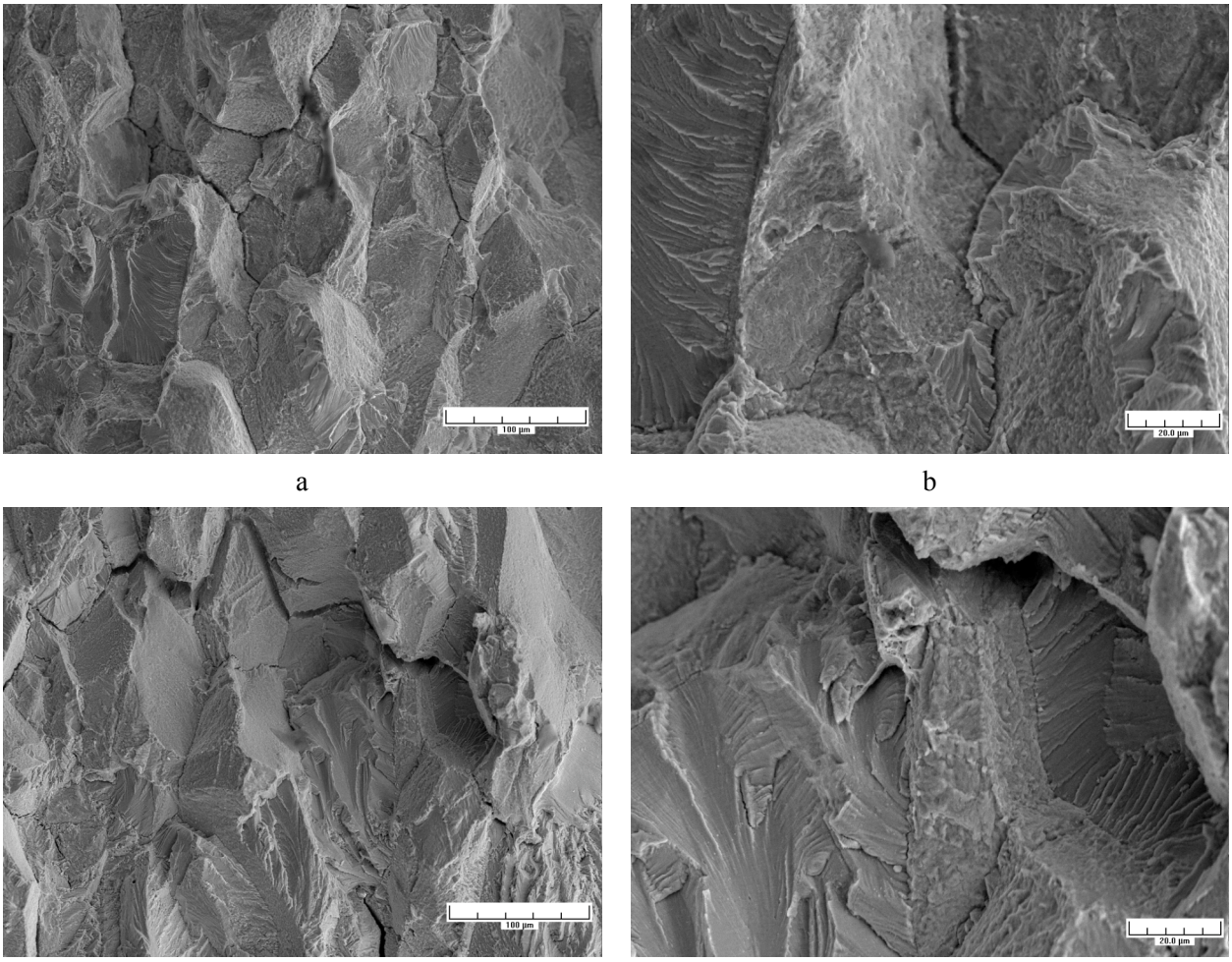

Figure 35. Low– (a, c) and high–magnification photomicrographs comparing the fracture surface in region IG–1 (a, b) and IG–2 (c, d).

The environmental enhancement of the CGR in the 30% CW Heat NX131031 in high–DO water appears to be a factor of 2–5 lower than that observed for MA material. This difference may be partially due to a change in the CGRs in air, e.g., the CGRs of 30% CW Alloy 600 in air seem to be somewhat lower than those for the MA material that have been used to plot the data in Fig. 36a. Taking into account lower CGRs of the CW alloy in air would result in the data for the cold-worked material in Fig. 36a shifting to the left. If the rates are decreased by a factor of 2, the growth rates of the 30% CW Alloy 600 would be comparable to those for the MA material. These results are counter to the general belief that cold work increases the susceptibility of Alloy 600 to environmentally assisted cracking in high–DO water at 289°C.

In Fig. 37 the results for Heat NX131031 are compared with the fatigue CGR for several other heats of Alloy 600 in high– and low–DO environments. In high–DO environments at 289°C, nearly all of the heats and heat treatment conditions show enhanced growth rates. The growth rates for MA Heat NX131031 are slightly higher than for the other heats of Alloy 600 that have been investigated.

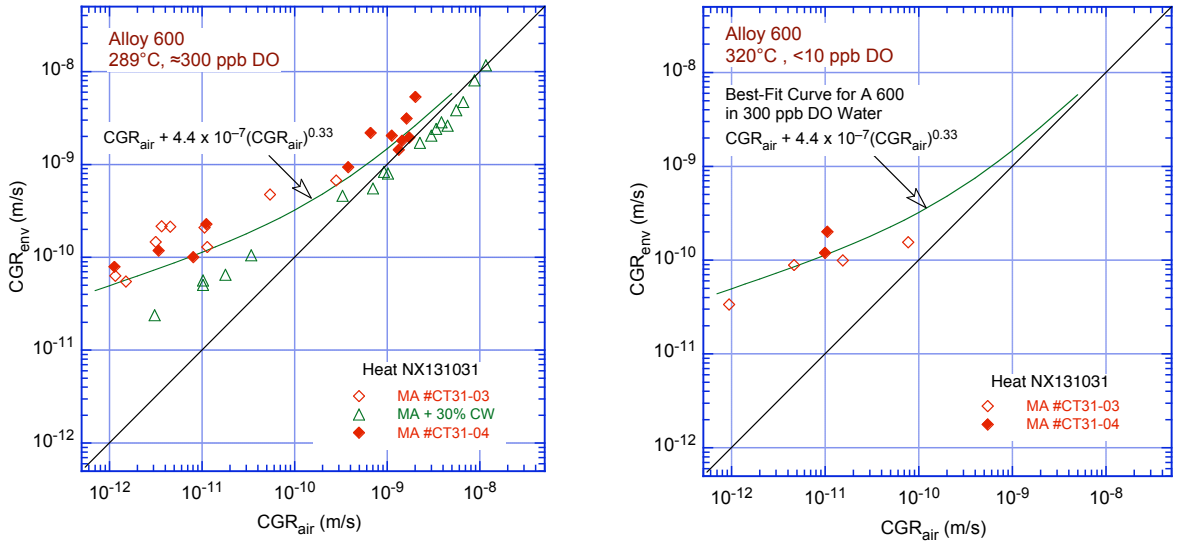

(a) (b)

Figure 36. Fatigue CGR data for mill–annealed and 30% cold worked Alloy 600 in high–purity water with (a) ≈300 ppb DO at 289°C and (b) ≈5 ppb DO at 320°C.

In contrast to the behavior in high–DO water, the environmental enhancement of CGRs of Alloy 600 in low–DO water seems much more variable from heat–to–heat of material. Environmental enhancement of growth rates was observed in both specimens of Heat NX131031 in low–DO high–purity water at 320°C, but other heats show little susceptibility to environmental enhancement. Steam generator tubing materials with high yield strength and/or low grain boundary coverage of carbides exhibit markedly greater susceptibility to environmentally assisted cracking. The correlation between susceptibility, yield strength, and grain boundary carbide coverage is not as well established for other material forms.

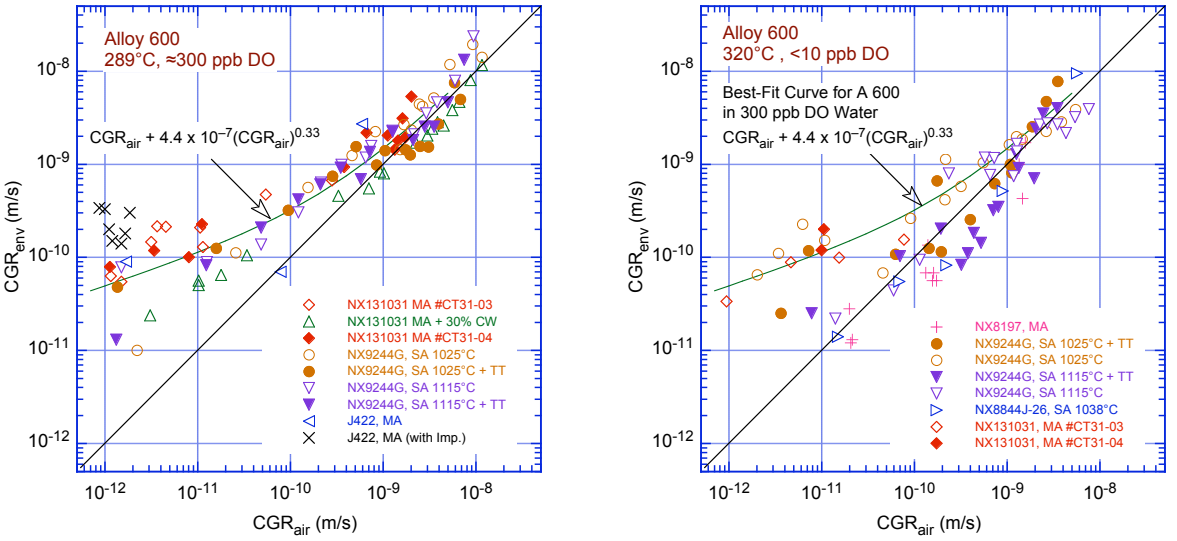

(a) (b)

Figure 37. Fatigue CGR data for several heats of Alloy 600 in high–purity water with (a) ≈300 ppb DO at 289°C and (b) <10 ppb DO at 320°C.

5.3.2 SCC Crack Growth Rates

The SCC CGRs for Heat NX131031, obtained with a trapezoidal waveform, in high–DO water at 289°C and low–DO water at 320°C are plotted as a function of applied K in Fig. 38a and b, respectively. The rates are similar to those observed under cyclic loading with $CGR_{air} \approx 10^{-12}$ m/s. For this material the CGRs in high–DO water at 289°C are comparable to those in low–DO water at 320°C.

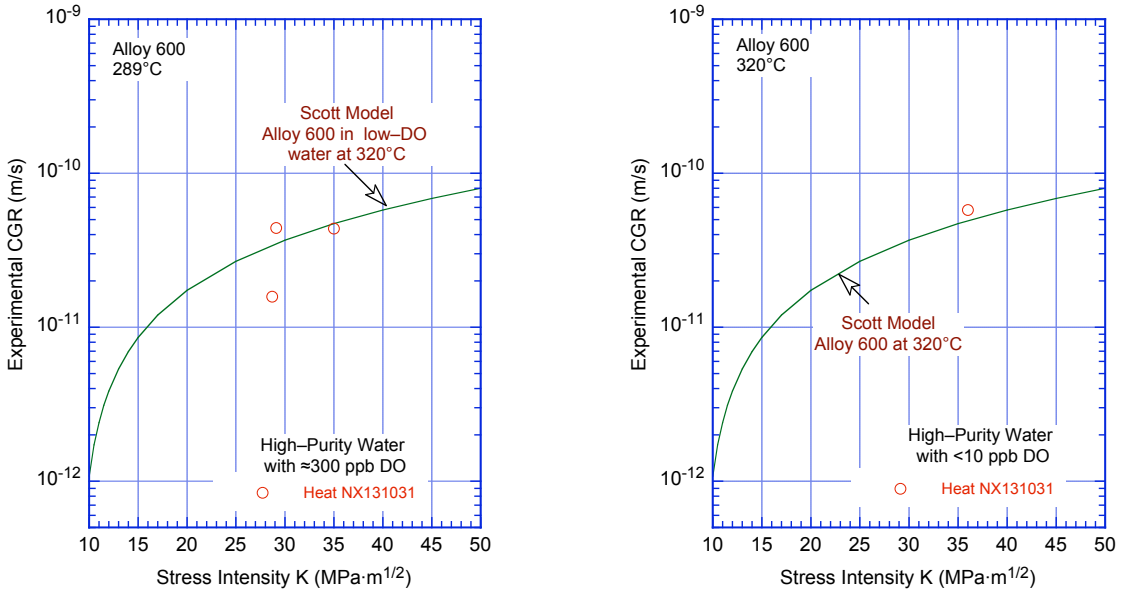

(a) (b)

Figure 38. SCC CGR data for mill–annealed Heat NX131031 of Alloy 600 in high–purity water with (a) ≈300 ppb DO at 289°C and (b) ≈5 ppb DO at 320°C.

The effect of the stress intensity K on SCC CGRs of Alloy 600 in PWR environments is generally represented by a relationship between crack growth rate CGR_{env} (m/s) and stress intensity factor K (Mpa $m^{1/2}$) originally developed by Scott to describe SCC crack growth rates in steam generator tubing

$$CGR_{env} = A(K - 9)^{1.16}. \quad (29)$$

The term A depends on the heat of material and temperature. The temperature dependence is usually assumed to follow an Arrhenius behavior with activation energy of 130 kJ/mole (31.1 kcal/mole). The CGR curve based on the Scott model is also shown in Fig. 38.

The SCC growth rate of Heat NX131031 in low–DO water can be compared with the rates of several other heats of Alloy 600 in PWR environments by comparing the values of the Scott model parameter A for the various heats of material. The CGRs for the various data sets were first normalized to 325°C, and then the best–fit parameter "A" in Eq. 29 was determined for each data set. The values were ordered and median ranks[125,126] were used to estimate the cumulative distribution of A for the population. This distribution can be fit reasonably well by a lognormal distribution with log mean –27.34. The distribution is plotted with a log scale for A in Fig. 39. The CGR of Heat NX131031 corresponds to 53rd percentile of the distribution for the sample of heats of Alloy 600, i.e., it is a typical heat.

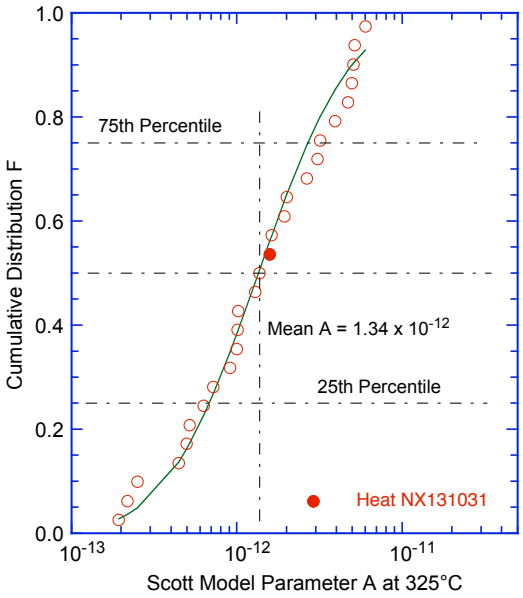

Figure 39.
Estimated cumulative distribution of the parameter A in the Scott model for CGR for heats of Alloy 600.

6 Summary

6.1 Environmental Effects on Fatigue ε–N Behavior

The existing fatigue ε–N data for carbon and low–alloy steels and wrought and cast austenitic SSs have been evaluated to define the effects of key material, loading, and environmental parameters on the fatigue lives of these steels. The fatigue lives of carbon and low–alloy steels and austenitic SSs are decreased in LWR environments; the magnitude of the reduction depends on temperature, strain rate, DO level in water, and, for carbon and low–alloy steels, S content in steel. For all steels, environmental effects on fatigue life are significant only when critical parameters (e.g., temperature, strain rate, DO level, and strain amplitude) meet certain threshold values. Environmental effects are moderate, e.g., less than a factor of 2 decrease in life, when any one of the threshold conditions is not satisfied. The threshold values of the critical parameters and the effects of other parameters (such as water conductivity, water flow rate, and material heat treatment) on the fatigue life of the steels are summarized.

Experimental data are presented on the effects of surface roughness on the fatigue life of carbon and low–alloy steels and austenitic stainless steels in air and LWR environments. Tests were conducted on specimens that were intentionally roughened, under controlled conditions, to an RMS surface roughness of 1.6 μm. For austenitic SSs, the fatigue life of roughened specimens is a factor of ≈3 lower than that of the smooth specimens in both air and low–DO water. In high–DO water, fatigue lives are comparable for smooth and roughened specimens. For carbon and low–alloy steels, the fatigue life of roughened specimens is lower than that of smooth specimens in air but is the same in high–DO water. In low–DO water, the fatigue life of the roughened specimens is slightly lower than that of smooth specimens. Because environmental effects on carbon and low–alloy steels are moderate in low–DO water, surface roughness is expected to influence fatigue life.

Statistical models are presented for estimating the fatigue life of carbon and low–alloy steels and wrought and cast austenitic SSs as a function of material, loading, and environmental parameters. Two approaches are presented for incorporating the effects of LWR environments into ASME Section III fatigue evaluations**.** In the first approach, environmentally adjusted fatigue design curves have been developed by adjusting the best–fit experimental curve for the effect of mean stress and by setting margins of 20 on cycles and 2 on strain to account for the uncertainties in life associated with material and loading conditions. The second approach considers the effects of reactor coolant environments on fatigue life in terms of an environmental correction factor F_{en}, which is the ratio of fatigue life in air at room temperature to that in water under reactor operating conditions.

Data available in the literature have been reviewed to evaluate the conservatism in the existing ASME Code fatigue evaluations. Much of the conservatism in these evaluations arises from current design procedures, e.g., stress analysis rules and cycle counting. However, the ASME Code permits alternative approaches, such as finite–element analyses, fatigue monitoring, and improved K_e factors, that can significantly decrease the conservatism in the current fatigue evaluation procedures.

Because of material variability, data scatter, and component size and surface, the fatigue life of actual components is different from that of laboratory test specimens under a similar loading history, and the mean ε–N curves for laboratory test specimens must be adjusted to obtain design curves for components. These design margins are another source of possible conservatism. The factors of 2 on stress and 20 on cycles used in the Code were intended to cover the effects of variables that can influence fatigue life but were not investigated in the tests which provided the data for the curves. Although these factors were intended to be somewhat conservative, they should not be considered safety margins because

they were intended to account for variables that are known to affect fatigue life. Data available in the literature have been reviewed to evaluate the margins on cycles and stress that are needed to account for the differences and uncertainties. In air, a factor of at least 12.5 on cycles with respect to the mean ε–N curve for laboratory test specimens is needed to account for the effects of data scatter and material variability, component size, surface finish, and loading sequence. In LWR environments, a factor of at least 19 on cycles with respect to the mean ε–N curve for laboratory test specimens is needed for austenitic SSs and at least 10 on cycles for carbon and low–alloy steels. Also, in air and LWR environments, a factor of 1.7 on stress is needed to account for the various differences and uncertainties.

The results indicate that the current ASME Code requirements of a factor of 2 on stress and 20 on cycle are quite reasonable, but do not contain excess conservatism that can be assumed to account for the effects of LWR environments. They thus provide appropriate design margins for the development of design curves from mean data curves for small specimens in LWR environments.

6.2 Irradiation–Assisted Stress Corrosion Cracking of Austenitic Stainless Steel in BWRs

Slow-strain-rate tensile (SSRT) tests were conducted in high-purity 289°C water on steels irradiated to ≈3 dpa in helium in the Halden Reactor. At ≈3 dpa, the bulk S content provided the best and the only good correlation with the susceptibility to intergranular (IG) SCC in 289°C water. Good resistance to IASCC was observed in Type 304 and 316 stainless steels that contain very low concentrations of S of ≈0.002 wt.% or less. The IASCC susceptibility of Type 304, 304L, 316, and 316L steels that contain >0.003 wt.% S increased drastically. Steels containing ≥0.008 wt.% were very susceptible at high fluence. These observations indicate that the deleterious effect of S plays a dominant role in the failure of core internal components at high fluence.

In contrast to Type 304 and 316 stainless steels, a low concentration of S of ≈0.001-0.002 wt.% does not necessarily render low-carbon Types 304L and 316L, or high-purity-grade steel resistant to IASCC. This indicates that high concentration of C is beneficial in reducing the deleterious effect of S and that threshold S concentration to ensure good IASCC resistance is lower in a low-carbon steel than in a high-carbon steel.

Evidence of grain-boundary segregation was observed by Auger electron spectroscopy on BWR neutron absorber tubes fabricated from two heats of Type 304 SS.

Crack growth tests have been performed in simulated BWR environments at ≈289°C on Type 304 SS (Heat C3) irradiated to 0.9 and 2.0 x 10^{21} n·cm^{-2} (1.35 and 3 dpa) and Type 316 SS (Heat C16) irradiated to 2.0 x 10^{21} n·cm^{-2} (3 dpa) at ≈288°C in a helium environment. The tests were conducted under cyclic loading with a slow/fast sawtooth waveform and long rise times or a trapezoidal waveform. The latter essentially represents constant load with periodic unloading and loading.

The results indicate significant enhancement of CGRs of irradiated steel in the NWC BWR environment, the CGRs of irradiated steels are a factor of ≈5 higher than the disposition curve proposed in NUREG–0313 for sensitized austenitic SSs in water with 8 ppm DO. Actual enhancement in same purity water is greater than 5. The CGRs of Type 304 SS irradiated to 1.35 and 3.0 dpa and of Type 316 SS irradiated to 3 dpa, are comparable.

In low–DO environment with low ECPs, the CGRs of the irradiated steels decreased by an order of magnitude in tests in which the K validity criterion was satisfied. For example, Heat C3 of Type 304 SS

irradiated to 1.35 dpa and Heat C16 of Type 316 SS irradiated to 3 dpa. No beneficial effect of decreased DO was observed for Heat C3 of Type 304 SS irradiated to 3 dpa, but in this case the applied K values during the low ECP portion of the test exceeded those required to meet the K validity criterion based on effective yield stress.

6.3 Irradiation–Assisted Cracking of Austenitic Stainless Steel in PWRs

A comprehensive irradiation experiment in BOR-60 Reactor is under progress to obtain a large number of tensile and disk specimens irradiated under PWR-like conditions at ≈325°C to 5, 10, and 40 dpa. Irradiation to ≈5 and ≈10 dpa has been completed.

Tests performed on the materials irradiated in the Halden BWR reactor may, however, give some insight into potential mechanisms for IASCC that is also relevant to PWRs. After exposure to the conditions of the SSRT test in BWR water, susceptibility to intergranular cracking in inert environment was determined by rapid bending in air at 23°C. Similar tests were also performed on hydrogen-charged specimens in vacuum. Both types of bend fracture exhibited similar characteristics suggesting that in both cases the failures occurred due to hydrogen-induced intergranular failure. However, steels that showed high susceptibility to IGSCC in 289°C water exhibited low susceptibility to intergranular cracking in the tests at 23°C air or vacuum, and vice versa. This indicates that although intergranular cracking in 23°C is dominated by H-induced embrittlement of ordinary grain boundaries, other processes control IASCC in 289°C water.

On the basis of this investigation, and studies on binary Ni–S and crack-tip microstructural characteristics of LWR core internal components reported in literature, an initial IASCC model based on a crack-tip grain-boundary process that involves S has been proposed. In this model, several processes play key role: i.e., grain-boundary segregation of Ni and S, formation of grain-boundary oxide in front of crack tip, formation of Ni– and S–rich thin films, and islands between the oxide and metal matrix, and disorder–induced melting or amorphization of the Ni–S thin films and islands at sufficiently high concentration of S.

6.4 Environmentally Assisted Cracking of Alloys 600 and 690 in LWR Water

The resistance of Ni alloys to EAC in simulated LWR environments is being evaluated. Crack growth tests are being conducted to establish the effects of alloy chemistry, material heat treatment, cold work, temperature, load ratio R, stress intensity K, and DO level on the CGRs of Ni alloys. During the current reporting period, a CGR test was completed on MA Alloy 600 (Heat NX131031) specimen in high–purity water at 289 and 320°C under various environmental and loading conditions. The results from this test are compared with data obtained earlier on the same heat of material in MA and MA plus 30% CW conditions.

In high–DO environment at 289°C, nearly all of the heats and heat treatment conditions that have been investigated show enhanced growth rates. The growth rates for MA Heat NX131031 are slightly higher than for the other heats of Alloy 600.

In contrast to the behavior in high–DO water, environmental enhancement of fatigue CGRs of Alloy 600 in low–DO water seems to depend on material condition, e.g., materials with high yield strength and/or low grain boundary coverage of carbides exhibit enhanced growth rates. Environmental enhancement of growth rates was observed in both specimens of Heat NX131031 in low–DO high–purity water at 320°C.

The SCC CGRs of Heat NX131031 in high–DO water at 289°C are comparable to those in low–DO water at 320°C. The results from the present study are compared with the data obtained on several other heats of Alloy 600. In a PWR environment, the CGR of Heat NX131031 corresponds to 53rd percentile of the distribution for the sample of heats of Alloy 600, i.e., Heat NX131031 represents an average heat.

References

1. Langer, B. F., "Design of Pressure Vessels for Low–Cycle Fatigue," ASME J. Basic Eng. 84, 389–402, 1962.

2. "Criteria of the ASME Boiler and Pressure Vessel Code for Design by Analysis in Sections III and VIII, Division 2," The American Society of Mechanical Engineers, New York, 1969.

3. Cooper, W. E., "The Initial Scope and Intent of the Section III Fatigue Design Procedure," Welding Research Council, Inc., Technical Information from Workshop on Cyclic Life and Environmental Effects in Nuclear Applications, Clearwater, Florida, January 20–21, 1992.

4. Ranganath, S., J. N. Kass, and J. D. Heald, "Fatigue Behavior of Carbon Steel Components in High–Temperature Water Environments," BWR Environmental Cracking Margins for Carbon Steel Piping, EPRI NP–2406, Electric Power Research Institute, Palo Alto, CA, Appendix 3, 1982.

5. Higuchi, M. and K. Iida, "Fatigue Strength Correction Factors for Carbon and Low–Alloy Steels in Oxygen–Containing High–Temperature Water," Nucl. Eng. Des. 129, 293–306, 1991.

6. Nagata, N., S. Sato, and Y. Katada, "Low–Cycle Fatigue Behavior of Pressure Vessel Steels in High–Temperature Pressurized Water," ISIJ Intl. 31 (1), 106–114, 1991.

7. Katada, Y., N. Nagata, and S. Sato, "Effect of Dissolved Oxygen Concentration on Fatigue Crack Growth Behavior of A533 B Steel in High–Temperature Water," ISIJ Intl. 33 (8), 877–883, 1993.

8. Kanasaki, H., M. Hayashi, K. Iida, and Y. Asada, "Effects of Temperature Change on Fatigue Life of Carbon Steel in High Temperature Water," in Fatigue and Crack Growth: Environmental Effects, Modeling Studies, and Design Considerations, PVP Vol. 306, S. Yukawa, ed., American Society of Mechanical Engineers, New York, pp. 117–122, 1995.

9. Nakao, G., H. Kanasaki, M. Higuchi, K. Iida, and Y. Asada, "Effects of Temperature and Dissolved Oxygen Content on Fatigue Life of Carbon and Low–Alloy Steels in LWR Water Environment," in Fatigue and Crack Growth: Environmental Effects, Modeling Studies, and Design Considerations, PVP Vol. 306, S. Yukawa, ed., American Society of Mechanical Engineers, New York, pp. 123–128, 1995.

10. Higuchi, M., K. Iida, and Y. Asada, "Effects of Strain Rate Change on Fatigue Life of Carbon Steel in High–Temperature Water," in Effects of the Environment on the Initiation of Crack Growth, ASTM STP 1298, W. A. Van Der Sluys, R. S. Piascik, and R. Zawierucha, eds., American Society for Testing and Materials, Philadelphia, pp. 216–231, 1997.

11. Iida, K., T. Bannai, M. Higuchi, K. Tsutsumi, and K. Sakaguchi, "Comparison of Japanese MITI Guideline and Other Methods for Evaluation of Environmental Fatigue Life Reduction," in Pressure Vessel and Piping Codes and Standards, PVP Vol. 419, M. D. Rana, ed., American Society of Mechanical Engineers, New York, pp. 73–82, 2001.

12. Chopra, O. K., and W. J. Shack, "Evaluation of Effects of LWR Coolant Environments on Fatigue Life of Carbon and Low–Alloy Steels," in Effects of the Environment on the Initiation of Crack Growth, ASTM STP 1298, W. A. Van Der Sluys, R. S. Piascik, and R. Zawierucha, eds., American Society for Testing and Materials, Philadelphia, pp. 247–266, 1997.

13. Chopra, O. K., and W. J. Shack, "Low–Cycle Fatigue of Piping and Pressure Vessel Steels in LWR Environments," Nucl. Eng. Des. 184, 49–76, 1998.

14. Chopra, O. K., and W. J. Shack, "Effects of LWR Coolant Environments on Fatigue Design Curves of Carbon and Low–Alloy Steels," NUREG/CR–6583, ANL–97/18, March 1998.

15. Chopra, O. K., and W. J. Shack, "Overview of Fatigue Crack Initiation in Carbon and Low–Alloy Steels in Light Water Reactor Environments," J. Pressure Vessel Technol. 121, 49–60, 1999.

16. Chopra, O. K., and J. Muscara, "Effects of Light Water Reactor Coolant Environments on Fatigue Crack Initiation in Piping and Pressure Vessel Steels," in Proc. 8th Intl. Conference on Nuclear Engineering, 2.08 LWR Materials Issue, Paper 8300, American Society of Mechanical Engineers, New York, 2000.

17. Chopra, O. K., and W. J. Shack, "Environmental Effects on Fatigue Crack Initiation in Piping and Pressure Vessel Steels," NUREG/CR–6717, ANL–00/27, May 2001.

18. Fujiwara, M., T. Endo, and H. Kanasaki, "Strain Rate Effects on the Low–Cycle Fatigue Strength of 304 Stainless Steel in High–Temperature Water Environment; Fatigue Life: Analysis and Prediction," in Proc. Intl. Conf. and Exposition on Fatigue, Corrosion Cracking, Fracture Mechanics, and Failure Analysis, ASM, Metals Park, OH, pp. 309–313, 1986.

19. Higuchi, M., and K. Iida, "Reduction in Low–Cycle Fatigue Life of Austenitic Stainless Steels in High–Temperature Water," in Pressure Vessel and Piping Codes and Standards, PVP Vol. 353, D. P. Jones, B. R. Newton, W. J. O'Donnell, R. Vecchio, G. A. Antaki, D. Bhavani, N. G. Cofie, and G. L. Hollinger, eds., American Society of Mechanical Engineers, New York, pp. 79–86, 1997.

20. Kanasaki, H., R. Umehara, H. Mizuta, and T. Suyama, "Effect of Strain Rate and Temperature Change on the Fatigue Life of Stainless Steel in PWR Primary Water," Trans. 14th Intl. Conf. on Structural Mechanics in Reactor Technology (SMiRT 14), Lyon, France, pp. 485–493, 1997.

21. Kanasaki, H., R. Umehara, H. Mizuta, and T. Suyama, "Fatigue Lives of Stainless Steels in PWR Primary Water," Trans. 14th Intl. Conf. on Structural Mechanics in Reactor Technology (SMiRT 14), Lyon, France, pp. 473–483, 1997.

22. Tsutsumi, K., H. Kanasaki, T. Umakoshi, T. Nakamura, S. Urata, H. Mizuta, and S. Nomoto, "Fatigue Life Reduction in PWR Water Environment for Stainless Steels," in Assessment Methodologies for Preventing Failure: Service Experience and Environmental Considerations, PVP Vol. 410-2, R. Mohan, ed., American Society of Mechanical Engineers, New York, pp. 23–34, 2000.

23. Tsutsumi, K., T. Dodo, H. Kanasaki, S. Nomoto, Y. Minami, and T. Nakamura, "Fatigue Behavior of Stainless Steel under Conditions of Changing Strain Rate in PWR Primary Water," in Pressure Vessel and Piping Codes and Standards, PVP Vol. 419, M. D. Rana, ed., American Society of Mechanical Engineers, New York, pp. 135–141, 2001.

24. Chopra, O. K., and D. J. Gavenda, "Effects of LWR Coolant Environments on Fatigue Lives of Austenitic Stainless Steels," J. Pressure Vessel Technol. 120, 116–121, 1998.

25. Chopra, O. K., and J. L. Smith, "Estimation of Fatigue Strain–Life Curves for Austenitic Stainless Steels in Light Water Reactor Environments," in Fatigue, Environmental Factors, and New Materials, PVP Vol. 374, H. S. Mehta, R. W. Swindeman, J. A. Todd, S. Yukawa, M. Zako, W. H. Bamford, M. Higuchi, E. Jones, H. Nickel, and S. Rahman, eds., American Society of Mechanical Engineers, New York, pp. 249–259, 1998.

26. Chopra, O. K., "Effects of LWR Coolant Environments on Fatigue Design Curves of Austenitic Stainless Steels," NUREG/CR–5704, ANL–98/31, 1999.

27. Chopra, O. K., "Mechanism and Estimation of Fatigue Crack Initiation in Austenitic Stainless Steels in LWR Environments," NUREG/CR–6787, ANL–01/25, 2002.

28. Chopra, O. K., "Development of Fatigue Design Curve for Austenitic Stainless Steels in LWR Environments: A Review," in Pressure Vessel and Piping Codes and Standards - 2002, PVP Vol. 439, R. D. Rana, ed., American Society of Mechanical Engineers, New York, pp. 119–132, 2002.

29. Smith, J. L., O. K. Chopra, and W. J. Shack, "Effect of Water Chemistry on the Fatigue Life of Austenitic Stainless Steels in LWR Environments," in Environmentally Assisted Cracking in Light Water Reactoirs, Semiannual Report, January 1999–June 1999, NUREG/CR–4667, Vol. 28, ANL–00/7, pp. 13–27, July 2000.

30. Hickling, J., "Strain–Induced Corrosion Cracking of Low–Alloy Reactor Pressure Vessel Steels under BWR Conditions," in Proc. of the Tenth Intl. Symp. on Environmental Degradation of Materials in Nuclear Power Systems–Water Reactors, The Minerals, Metals, and Materials Society, Warrendale, PA, CD-ROM, paper #0156, 2001).

31. Solomon, H. D., R. E. DeLair, and A. D. Unruh, "Crack Initiation in Low–Alloy Steel in High–Temperature Water," in Effects of the Environment on the Initiation of Crack Growth, ASTM STP 1298, W. A. Van Der Sluys, R. S. Piascik, and R. Zawierucha, eds., American Society for Testing and Materials, Philadelphia, pp. 135–149, 1997.

32. Solomon, H. D., R. E. DeLair, and E. Tolksdorf, "LCF Crack Initiation in WB36 in High Temperature Water" in Proc. of the Ninth Intl. Symp. on Environmental Degradation of Materials in Nuclear Power Systems–Water Reactors, Steve Bruemmer, Peter Ford, and Gary Was, eds., The Minerals, Metals, and Materials Society, Warrendale, PA, pp. 865-872, 1999.

33. Hirano, A., M. Yamamoto, K. Sakaguchi, K. Iida, and T. Shoji, "Effects of Water Flow Rate on Fatigue Life of Carbon Steel in High–Temperature Pure Water Environment," in Assessment Methodologies for Predicting Failure: Service Experience and Environmental Considerations, PVP Vol. 410–2, R. Mohan, ed., American Society of Mechanical Engineers, New York, pp. 13–18, 2000.

34. Hirano, A., M. Yamamoto, K. Sakaguchi, T. Shoji, and K. Iida, "Effects of Water Flow Rate on Fatigue Life of Ferritic and Austenitic Steels in Simulated LWR Environment," in Pressure Vessel and Piping Codes and Standards - 2002, PVP Vol. 439, R. D. Rana, ed., American Society of Mechanical Engineers, New York, pp. 143–150, 2002.

35. Lenz, E., N. Wieling, and H. Muenster, “Influence of Variation of Flow Rates and Temperature on the Cyclic Crack Growth Rate under BWR Conditions,” in Environmental Degradation of Materials in Nuclear Power Systems – Water Reactors, The Metallurgical Society, Warrendale, PA, 1988.

36. Amzallag, C., P. Rabbe, G. Gallet, H.–P. Lieurade, “Influence des Conditions de Sollicitation Sur le Comportement en Fatigue Oligocyclique D'aciers Inoxydables Austénitiques,” Memoires Scientifiques Revue Metallurgie Mars, pp. 161–173, 1978.

37. Jaske, C. E., and W. J. O'Donnell, “Fatigue Design Criteria for Pressure Vessel Alloys,” Trans. ASME J. Pressure Vessel Technol. 99, 584–592, 1977.

38. Hale, D. A., S. A. Wilson, E. Kiss, and A. J. Gianuzzi, “Low Cycle Fatigue Evaluation of Primary Piping Materials in a BWR Environment,” GEAP–20244, U.S. Nuclear Regulatory Commission, 1977.

39. Mehta, H. S., and S. R. Gosselin, “Environmental Factor Approach to Account for Water Effects in Pressure Vessel and Piping Fatigue Evaluations,” Nucl. Eng. Des. 181, 175–197, 1998.

40. Mehta, H. S., “An Update on the EPRI/GE Environmental Fatigue Evaluation Methodology and its Applications,” in Probabilistic and Environmental Aspects of Fracture and Fatigues, PVP Vol. 386, S. Rahman, ed., American Society of Mechanical Engineers, New York, pp. 183–193, 1999.

41. Wire, G. L., T. R. Leax, and J. T. Kandra, “Mean Stress and Environmental Effects on Fatigue in Type 304 Stainless Steel,” Probabilistic and Environmental Aspects of Fracture and Fatigues, PVP Vol. 386, S. Rahman, ed., American Society of Mechanical Engineers, New York, pp. 213–228, 1999.

42. Mayfield, M. E., E. C. Rodabaugh, and R. J. Eiber, “A Comparison of Fatigue Test Data on Piping with the ASME Code Fatigue Evaluation Procedure,” ASME Paper 79–PVP–92, American Society of Mechanical Engineers, New York, 1979.

43. Heald, J. D., and E. Kiss, “Low Cycle Fatigue of Nuclear Pipe Components,” J. Pressure Vessel Technol. 74, PVP–5, 1–6, 1974.

44. Deardorff, A. F., and J. K. Smith, “Evaluation of Conservatisms and Environmental Effects in ASME Code, Section III, Class 1 Fatigue Analysis,” SAND94–0187, prepared by Structural Integrity Associates, San Jose, CA, under contract to Sandia National Laboratories, Albuquerque, NM, 1994.

45. Kooistra, L. F., E. A. Lange, and A. G. Pickett, “Full–Size Pressure Vessel Testing and Its Application to Design,” J. Eng. Power 86, 419–428, 1964.

46. Scott, P. M.. and G. M. Wilkowski, “A Comparison of Recent Full–Scale Component Fatigue Data with the ASME Section III Fatigue Design Curves,” Fatigue and Crack Growth: Environmental Effects, Modeling Studies, and Design Considerations, PVP Vol. 306, S. Yukawa, ed., American Society of Mechanical Engineers, New York, pp. 129–138, 1995.

47. Hechmer, J., "Evaluation Methods for Fatigue - A PVRC Project," Fatigue, Environmental Factors, and New Materials, PVP Vol. 374, H. S. Mehta, R. W. Swindeman, J. A. Todd, S. Yukawa, M. Zako, W. H. Bamford, M. Higuchi, E. Jones, H. Nickel, and S. Rahman, eds., American Society of Mechanical Engineers, New York, pp. 191–199, 1998.

48. Johnson, L. G., "The Median Ranks of Sample Values in Their Population with an Application to Certain Fatigue Studies," Ind. Math. 2, 1–9, 1951.

49. Lipson, C., and N. J. Sheth, Statistical Design and Analysis of Engineering Experiments, McGraw Hill, New York, 1973.

50. Beck, J., and K. Arnold, "Parameter Estimation in Engineering and Science," J. Wiley, New York, 1977.

51. Maiya, P. S., and D. E. Busch, "Effect of Surface Roughness on Low–Cycle Fatigue Behavior of Type 304 Stainless Steel," Met. Trans. 6A, 1761–1766, 1975.

52. Maiya, P. S., "Effect of Surface Roughness and Strain Range on Low–Cycle Fatigue Behavior of Type 304 Stainless Steel," Scripta Metall. 9, 1277–1282, 1975.

53. Stout, K. J., "Surface Roughness – Measurement, Interpretation, and Significance of Data," Mater. Eng. 2, 287–295, 1981.

54. Iida, K., "A Study of Surface Finish Effect Factor in ASME B & PV Code Section III," Pressure Vessel Technology, Vol. 2, L. Cengdian and R. W. Nichols, eds., Pergamon Press, New York, pp. 727–734, 1989.

55. Gavenda, D. J., P. R. Luebbers, and O. K. Chopra, "Crack Initiation and Crack Growth Behavior of Carbon and Low–Alloy Steels," Fatigue and Fracture 1, Vol. 350, S. Rahman, K. K. Yoon, S. Bhandari, R. Warke, and J. M. Bloom, eds., American Society of Mechanical Engineers, New York, pp. 243–255, 1997.

56. Chopra, O. K., "Mechanism of Fatigue Crack Initiation in Austenitic Stainless Steels in LWR Environments," Pressure Vessel and Piping Codes and Standards - 2002, PVP Vol. 439, R. D. Rana, ed., American Society of Mechanical Engineers, New York, pp. 133–142, 2002.

57. Pompetzki, M. A., T. H. Topper, and D. L. DuQuesnay, "The Effect of Compressive Underloads and Tensile Overloads on Fatigue Damage Accumulation in SAE 1045 Steel," Int. J. Fatigue 12 (3), 207–213, 1990.

58. Conle, A., and T. H. Topper, "Evaluation of Small Cycle Omission Criteria for Shortening of Fatigue Service Histories," Int. J. Fatigue 1, 23–28, 1979.

59. Conle, A., and T. H. Topper, "Overstrain Effects During Variable Amplitude Service History Testing," Int. J. Fatigue 2, 130–136, 1980.

60. Nian, Li, and Du Bai–Ping, "Effect of Monotonic and Cyclic Prestrain on the Fatigue Threshold in Medium–Carbon Steels," Int. J. Fatigue 14 (1), 41–44, 1992.

61. Manjoine, M. J., “Fatigue Damage Models for Annealed Type 304 Stainless Steel under Complex Strain Histories,” Trans. 6th Intl. Conf. on Structural Mechanics in Reactor Technology (SMiRT), Vol. L, 8/1, North–Holland Publishing Co., pp. 1–13, 1981.

62. Nian, Li, and Du Bai–Ping, “The Effect of Low–Stress High–Cycle Fatigue on the Microstructure and Fatigue Threshold of a 40Cr Steel,” Int. J. Fatigue 17 (1), 43–48, 1995.

63. Indig, M. E., J. L. Nelson, and G. P. Wozadlo, “Investigation of Protection Potential against IASCC,” Proc. 5th Intl. Symp. on Environmental Degradation of Materials in Nuclear Power Systems – Water Reactors, D. Cubicciotti, E. P. Simonen, and R. Gold, eds., American Nuclear Society, LaGrange Park, IL, pp. 941-947, 1992.

64. Kodama, M., S. Nishimura, J. Morisawa, S. Shima, S. Suzuki, and M. Yamamoto, “Effects of Fluence and Dissolved Oxygen on IASCC in Austenitic Stainless Steels,” Proc. 5th Intl. Symp. on Environmental Degradation of Materials in Nuclear Power Systems – Water Reactors, D. Cubicciotti, E. P. Simonen, and R. Gold, eds., American Nuclear Society, LaGrange Park, IL, pp. 948-954, 1992.

65. Chung, H. M., W. E. Ruther, J. E. Sanecki, A. G. Hins, and T. F. Kassner, “Effects of Water Chemistry on Intergranular Cracking of Irradiated Austenitic Stainless Steels,” Proc. 7th Intl. Symp. on Environmental Degradation of Materials in Nuclear Power Systems - Water Reactors, G. Airey et al., eds., NACE International, Houston, 1995, pp. 1133-1143.

66. Garzarolli, F., P. Dewes, R. Hahn, and J. L. Nelson, “Deformability of High-Purity Stainless Steels and Ni–Base Alloys in the Core of a PWR,” Proc. 6th Intl. Symp. on Environmental Degradation of Materials in Nuclear Power Systems - Water Reactors, R. E. Gold and E. P. Simonen, eds., The Minerals, Metals, and Materials Society, Warrendale, PA, 1993, pp. 607-613.

67. Kanasaki, H., T. Okubo, I. Satoh, M. Koyama, T. R. Mager, and R. G. Lott, “Fatigue and Stress Corrosion Cracking Behavior of Irradiated Stainless Steels in PWR Primary Water,” Proc. 5th Intl. Conf. on Nuclear Engineering, March 26-30, 1997, Nice, France.

68. Fukuya, K., K. Fuji, M. Nakano, N. Nakajima, and M. Kodama, “Stress Corrosion Cracking on Cold-Worked Stainless Steels Irradiated to High Fluence,” Proc. 10th Intl. Conf. on Environmental Degradation of Materials in Nuclear Power Systems - Water Reactors, August 5-9, 2001, Lake Tahoe, Nevada, G. S. Was and J. L. Nelson, eds., NACE International CD-ROM.

69. Jacobs, A. J., G. P. Wozadlo, K. Nakata, T. Yoshida, and I. Masaoka, "Radiation Effects on the Stress Corrosion and Other Selected Properties of Type-304 and Type-316 Stainless Steels,” Proc. 3rd Intl. Symp. Environmental Degradation of Materials in Nuclear Power Systems – Water Reactors, G. J. Theus and J. R. Weeks, eds., The Metallurgical Society, Warrendale, PA, pp. 673-680, 1988.

70. Garzarolli, F., D. Alter, P. Dewes, and J. L. Nelson, “Deformability of Austenitic Stainless Steels and Ni–Base Alloys,” Proc. 3th Intl. Symp. on Environmental Degradation of Materials in Nuclear Power Systems - Water Reactors, G. J Theus and J. R. Weeks, eds., The Metallurgical Society, Warrendale, PA, pp. 657-664, 1988.

71. Fukuya, K., S. Shima, K. Nakata, S. Kasahara, A. J. Jacobs, G. P. Wozadlo, S. Suzuki, and M. Kitamura, "Mechanical Properties and IASCC Susceptibility in Irradiated Stainless Steels," Proc. 6th Intl. Symp. on Environmental Degradation of Materials in Nuclear Power Systems - Water Reactors, R. E. Gold, and E. P. Simonen, eds., The Minerals, Metals, and Materials Society, Warrendale, PA, pp. 565-572, 1993.

72. Chung, H. M., W. E. Ruther, J. E. Sanecki, A. G. Hins, and T. F. Kassner, "Stress Corrosion Cracking Susceptibility of Irradiated Type 304 Stainless Steels," Effects of Radiation on Materials: 16th Int. Symp., ASTM STP 1175, A. S. Kumar, D. S. Gelles, R. K. Nanstad, and T. A. Little, eds., American Society for Testing and Materials, Philadelphia, pp. 851-869, 1993.

73. Chung, H. M., W. E. Ruther, J. E. Sanecki, and T. F. Kassner, "Grain-Boundary Microchemistry and Intergranular Cracking of Irradiated Austenitic Stainless Steels," Proc. 6th Intl. Symp. on Environmental Degradation of Materials in Nuclear Power Systems - Water Reactors, R. E. Gold, and E. P. Simonen, eds., The Minerals, Metals, and Materials Society, Warrendale, PA, pp. 511-519, 1993.

74. Cookson, J. M., D. L. Damcott, G. S. Was, and P. L. Anderson, "The Role of Microchemical and Microstructural Effects in the IASCC of High-Purity Austenitic Stainless Steels," Proc. 6th Intl. Symp. on Environmental Degradation of Materials in Nuclear Power Systems - Water Reactors, R. E. Gold, and E. P. Simonen, eds., The Minerals, Metals, and Materials Society, Warrendale, PA, pp. 573-580, 1993.

75. Kodama, M., R. Katsura, J. Morisawa, S. Nishimura, S. Suzuki, K. Asano, K. Fukuya, and K. Nakata, "IASCC Susceptibility of Austenitic Stainless Steels Irradiated to High Neutron Fluence," Proc. 6th Intl. Symp. on Environmental Degradation of Materials in Nuclear Power Systems - Water Reactors, R. E. Gold and E. P. Simonen, eds., The Minerals, Metals, and Materials Society, Warrendale, PA, pp. 583-588, 1993.

76. Jacobs, A. J., G. P. Wozadlo, T. Okada, S. Kawano, K. Nakata, S. Kasahara, and S. Suzuki, "The Correlation of Grain Boundary Composition in Irradiated Stainless Steels with IASCC Resistance," Proc. 6th Intl. Symp. on Environmental Degradation of Materials in Nuclear Power Systems - Water Reactors, R. E. Gold and E. P. Simonen, eds., The Minerals, Metals, and Materials Society, Warrendale, PA, pp. 597-604, 1993.

77. Kasahara, S., K. Nakata, K. Fukuya, S. Shima, A. J. Jacobs, G. P. Wozadlo, and S. Suzuki, "The Effects of Minor Elements on IASCC Susceptibility in Austenitic Stainless Steels Irradiated with Neutrons," Proc. 6th Intl. Symp. on Environmental Degradation of Materials in Nuclear Power Systems - Water Reactors, R. E. Gold and E. P. Simonen, eds., The Minerals, Metals, and Materials Society, Warrendale, PA, pp. 615-623, 1993.

78. Kodama, M., J. Morisawa, S. Nishimura, K. Asano, S. Shima, and K. Nakata, J. Nucl. Mater., 212–215, 1509, 1994.

79. Tsukada, T., and Y. Miwa, "Stress Corrosion Cracking of Neutron Irradiated Stainless Steels," Proc. 7th Int. Symp. on Environmental Degradation of Materials in Nuclear Power Systems - Water Reactors, G. Airey et al., eds., NACE International, Houston, pp. 1009–1018, 1995.

80. Jenssen, A., and L. G. Ljungberg, "Irradiation-Assisted Stress Corrosion Cracking - Postirradiation CERT Tests of Stainless Steels in a BWR Test Loop," Proc. 7th Intl. Symp. on Environmental Degradation of Materials in Nuclear Power Systems - Water Reactors, G. Airey et al., eds., NACE International, Houston, pp. 1043–1052, 1995.

81. Garzarolli, F., P. Dewes, R. Hahn, and J. L. Nelson, "In-Reactor Testing of IASCC Resistant Stainless Steels," Proc. 7th Intl. Symp. on Environmental Degradation of Materials in Nuclear Power Systems - Water Reactors, G. Airey et al., eds., NACE International, Houston, pp. 1055–1065, 1995.

82. Chung, H. M., W. E. Ruther, J. E. Sanecki, A. G. Hins, N. J. Zaluzec, and T. F. Kassner, J. Nucl. Mater. 239, 61, 1996.

83. Tanaka, Y., S. Suzuki, K. Fukuya, H. Sakamoto, M. Kodama, S. Nishimura, K. Nakata, and T. Kato, "IASCC Susceptibility of Type 304, 304L, and 316 Stainless Steels," Proc. 8th Int. Symp. on Environmental Degradation of Materials in Nuclear Power Systems - Water Reactors, S. M. Bruemmer, ed., American Nuclear Society, LaGrange Park, IL, pp. 803-811, 1997.

84. Chung, H. M., R. V. Strain, and W. J. Shack, "Irradiation-Assisted Stress Corrosion Cracking of Model Austenitic Stainless Steel Alloys," CD-ROM, Proc. 10th Intl. Conf. on Environmental Degradation of Materials in Nuclear Power Systems - Water Reactors, Lake Tahoe, NV, Aug. 2001.

85. Chung, H. M., R. V. Strain, and R. W. Clark, "Irradiation-Assisted Stress Corrosion Cracking of Austenitic Stainless Steel in BWRs," Environmentally Assisted Cracking in Light Water Reactors, NUREG/CR-4667, Vol. 32, ANL-02/33, Annual Report, Argonne National Laboratory, pp.19-28, June 2003.

86. Andresen, P. L., and C. L. Briant, "The Role of S, P, and N Segregation in Intergranular Environmental Cracking of Stainless Steels in High-Temperature Water," Proc. 3rd Intl. Symp. Environmental Degradation of Materials in Nuclear Power Systems – Water Reactors, G. J. Theus and J. R. Weeks, eds., The Metallurgical Society, Warrendale, PA, pp. 371-381, 1988.

87. Bruemmer, S. M., et al., "Critical Issue Reviews for the Understanding and Evaluation of Irradiation–Assisted Stress Corrosion Cracking," EPRI TR–107159, Electric Power Research Institute, Palo Alto, CA, 1996.

88. Herrera, M. L., et al., "Evaluation of the Effects of Irradiation on the Fracture Toughness of BWR Internal Components," Proc. ASME/JSME 4th Intl. Conf. on Nucl. Eng. (ICONE–4), Vol. 5, p. 245, Eds., A. S. Rao, R. M. Duffey, and D. Elias, American Society of Mechanical Engineers, New York, 1996.

89. Mills, W. J., "Fracture Toughness of Type 304 and 316 Stainless Steels and their Welds," Intl. Mater. Rev., 42, 45, 1997.

90. Kanasaki, H., I. Satoh, M. Koyama, T. Okubo, T. R. Mager, and R. G. Lott, "Fatigue and Stress Corrosion Cracking Behaviors of Irradiated Stainless Steels in PWR Primary Water," Proc. 5th Intl. Conf. on Nuclear Engineering, ICONE5-2372, p. 1, 1997.

91. Andresen, P. L., F. P. Ford, S. M. Murphy, and J. M. Perks, "State of Knowledge of Radiation Effects on Environmental Cracking in Light Water Reactor Core Materials," Proc. 4th Intl. Symp. on Environmental Degradation of Materials in Nuclear Power Systems – Water Reactors, p. 1.83, NACE, Houston, TX, 1990.

92. Jenssen, A., and L. G. Ljungberg, "Irradiation Assisted Stress Corrosion Cracking of Stainless Alloys in BWR Normal Water Chemistry and Hydrogen Water Chemistry," Proc. Sixth Intl. Symp. on Environmental Degradation of Materials in Nuclear Power Systems – Water Reactors, p. 547, Eds., R. E. Gold and E. P. Simonen, The Minerals, Metals & Materials Society, Warrendale, PA, 1993.

93. Gordon, G. M., and K. S. Brown, "Dependence of Creviced BWR Component IGSCC Behavior on Coolant Chemistry," Proc. 4th Intl. Symp. on Environmental Degradation of Materials in Nuclear Power Systems – Water Reactors, p. 14.46, NACE, Houston, TX, 1990.

94. Garzarolli, F., D. Alter, and P. Dewes, "Deformability of Austenitic Stainless Steels and Nickel–Base Alloys in the Core of a Boiling and a Pressurized Water Reactor," Proc. Intl. Symp. on Environmental Degradation of Materials in Nuclear Power Systems – Water Reactors, p. 131, American Nuclear Society, La Grange Park, IL, 1986.

95. Kodama, M., et al., "IASCC Susceptibility of Austenitic Stainless Steels Irradiated to High Neutron Fluence, " Proc. Sixth Intl. Symp. on Environmental Degradation of Materials in Nuclear Power Systems – Water Reactors, p. 583, Eds., R. E. Gold and E. P. Simonen, The Minerals, Metals & Materials Society, Warrendale, PA, 1993.

96. Kodama, M., et al., "Effects of Fluence and Dissolved Oxygen on IASCC in Austenitic Stainless Steels, " Proc. Fifth Intl. Symp. on Environmental Degradation of Materials in Nuclear Power Systems – Water Reactors, p. 948, American Nuclear Society, La Grange Park, IL, 1991.

97. Clark, W. L., and A. J. Jacobs, "Effect of Radiation Environment on SCC of Austenitic Materials," Proc. First Intl. Symp. on Environmental Degradation of Materials in Nuclear Power Systems – Water Reactors, p. 451, NACE, Houston, TX, 1983.

98. Jenssen, A., and L. G. Ljungberg, "Irradiation Assisted Stress Corrosion Cracking of Stainless Alloys in BWR Normal Water Chemistry and Hydrogen Water Chemistry," Proc. Sixth Intl. Symp. on Environmental Degradation of Materials in Nuclear Power Systems – Water Reactors, p. 547, Eds., R. E. Gold and E. P. Simonen, The Minerals, Metals & Materials Society, Warrendale, PA, 1993.

99. Jenssen, A., and L. G. Ljungberg, "Irradiation Assisted Stress Corrosion Cracking: Post Irradiation CERT Tests of Stainless Steels in a BWR Test Loop," Proc. Seventh Intl. Symp. on Environmental Degradation of Materials in Nuclear Power Systems – Water Reactors, p. 1043, Eds., G. Airey et al., NACE, Houston, TX, 1995.

100. Andresen, P. L., and F. P. Ford, "Irradiation Assisted Stress Corrosion Cracking: from Modeling and Prediction on Laboratory & In–Core Response to Component Life Prediction," Corrosion 95, Paper No. 419, NACE, Houston, 1995.

101. Gruber, E. E., and O. K. Chopra, "Fracture Toughness J–R Test of Austenitic Stainless Steels Irradiated in the Halden Reactor," Environmentally Assisted Cracking in Light Water Reactors Semiannual Report January–June 2000, NUREG/CR–4667, Vol. 30, ANL–01/08, p. 34, June 2001.

102. Chung, H. M., W. E. Ruther, R. V. Strain, and W. J. Shack, "Irradiated–Assisted Stress Corrosion Cracking of Model Austenitic Stainless Steel Alloys," NUREG/CR–6687, ANL–00/21, Oct. 2000.

103. Chung, H. M., R. V. Strain, and R. W. Clark, "Slow–Strain–Rate Tensile Test of Model Austenitic Stainless Steels Irradiated in the Halden Reactor," Environmentally Assisted Cracking in Light Water Reactors, Annual Report January–December 2001, NUREG/CR–4667, Vol. 32, ANL–02/33, p. 19, 2003.

104. Andresen, P. L., "Similarity of Cold Work and Radiation Hardening in Enhancing Yield Strength and SCC Growth of Stainless Steel in Hot Water," Corrosion 02, Paper 02509, NACE, Houston, 2002.

105. Shack, W. J., and T. F. Kassner, "Review of Environmental Effects on Fatigue Crack Growth of Austenitic Stainless Steels," NUREG/CR–6176, ANL–94/1, May 1994.

106. James, L. A., and D. P. Jones, "Fatigue Crack Growth Correlation for Austenitic Stainless Steels in Air," Proc. Conf. on Predictive Capabilities in Environmentally–Assisted Cracking, PVP Vol. 99, p. 363, Ed., R. Rungta, American Society of Mechanical Engineers, New York, 1985.

107. Hazelton, W. S., and W. H. Koo, "Technical Report on Material Selection and Processing Guidelines for BWR Coolant Pressure Boundary Piping," Final Report, NUREG–0313, Rev. 2, 1988.

108. Heuer, J. K., P. R. Okamoto, N. Q. Lam, J. F. Stubbins, "Disorder-Induced Melting in Nickel: Implication to Intergranular Sulfur Embrittlement," J. Nucl. Mater. 301, 129-141, 2002.

109. Okamoto, P. R., J. K. Heuer, and N. Q. Lam, "Is Segregation-Induced Grain Boundary Embrittlement a Polymorphous Melting Process?" in CD-ROM, Proc. 2003 TMS Spring Meeting, San Diego, CA, 2003.

110. Dumbill, S., "Examination of Stress Corrosion Crack Tip Microstructures in Stainless Steel," SKI Report 01:35, Swedish Nuclear Power Inspectorate, September 2001.

111. Thomas, L., and S. Bruemmer, "Analytical Transmission Microscopy, ATEM) Characterization of Stress Corrosion Cracks in LWR-Irradiated Austenitic Stainless Steel Components," EPRI-1003422, Electric Power Research Institute, Palo Alto, CA, May 2002.

112. Ashby, M. F., and F. Spaegen, "A New Model for the Structure of Grain Boundaries: Packing of Polyhedra," Scripta Met. 12, 193-195, 1978.

113. Ruther, W. E., W. K. Soppet, and T. F. Kassner, "Corrosion Fatigue of Alloys 600 and 690 in Simulated LWR Environments," NUREG/CR–6383, ANL–95/37, April 1996.

114. Ruther, W. E., W. K. Soppet, and T. F. Kassner, "Environmentally Assisted Cracking of Alloys 600 and 690 in Simulated LWR Water," Environmentally Assisted Cracking in Light Water Reactors, Semiannual Report, July 1997–December 1997, NUREG/CR–4667 Vol. 25, ANL–98/18, pp. 42–75, Sept. 1998.

115. Ruther, W. E., W. K. Soppet, T. F. Kassner, and W. J. Shack, "Environmentally Assisted Cracking of Alloys 600 and 690 in Simulated LWR Water," Environmentally Assisted Cracking in Light Water Reactors, Semiannual Report, January 1998–July 1998, NUREG/CR–4667 Vol. 26, ANL–98/18, pp. 25–32, March 1999.

116. Ruther, W. E., W. K. Soppet, T. F. Kassner, and W. J. Shack, "Environmentally Assisted Cracking of Alloys 600 and 690 in Simulated LWR Water," Environmentally Assisted Cracking in Light Water Reactors, Semiannual Report, July 1998–December 1998, NUREG/CR–4667 Vol. 27, ANL–99/11, pp. 45-54, October 1999.

117. Soppet, W. K., O. K. Chopra, and W. J. Shack, "Environmentally Assisted Cracking of Alloys 600 and 690 in Simulated LWR Water," Environmentally Assisted Cracking in Light Water Reactors, Semiannual Report, July 1999–December 1999, NUREG/CR–4667 Vol. 29, ANL–00/23, pp. 39-45, November 2000.

118. Chopra, O. K., W. K. Soppet, and W. J. Shack, "Effects of Alloy Chemistry, Cold Work, and Water Chemistry on Corrosion Fatigue and Stress Corrosion Cracking of Nickel Alloys and Welds," NUREG/CR–6721, ANL–01/07, April 2001.

119. Soppet, W. K., O. K. Chopra, and W. J. Shack, "Environmentally Assisted Cracking of Alloys 600 and 690 in Simulated LWR Water," Environmentally Assisted Cracking in Light Water Reactors, Semiannual Report, July 2000–December 2000, NUREG/CR–4667 Vol. 31, ANL–01/09, pp. 39-48, April 2002.

120. Soppet, W. K., O. K. Chopra, and W. J. Shack, "Cracking of Nickel Alloys and Weldments," Environmentally Assisted Cracking in Light Water Reactors, Annual Report, January–December 2001, NUREG/CR–4667 Vol. 32, ANL–02/33, pp. 49-56, June 2003.

121. Andresen, P. L., T. M. Angeliu, L. M. Young, W. R. Catlin, and R. M. Horn, "Mechanisms and Kinetics of SCC in Stainless Steels," Proc. 10th Intl. Symp. on Environmental Degradation of Materials in Nuclear Power Systems – Water Reactors, NACE International, Houston, 2001.

122. Rebak, R. B., A. R. McIlree, and Szklarska-Smialowska, "Effects of pH and Stress Intensity on Crack Growth Rate in Alloy 600 in Lithiated + Borated Water at High Temperatures," Proc. of the 5th Intl. Symp. on Environmental Degradation of Materials in Nuclear Power Systems–Water Reactors, American Nuclear Society, La Grange Park, IL, pp. 511-517, 1991.

123. Cassagne, T., and A. Gelpi, "Crack Growth Rate Measurements on Alloy 600 Steam Generator Tubing in Primary and Hydrogenated AVT Water," Proc. of the Sixth Intl. Symp. on Environmental Degradation of Materials in Nuclear Power Systems–Water Reactors, R. E. Gold and E. P. Simonen, eds., The Minerals, Metals, and Materials Society, Warrendale, PA, pp. 679-685, 1993.

124. Vaillant, F., C. Amzallag, and J. Champredonde, "Crack Growth Rate Measurements of Alloy 600 Vessel Head Penetrations," Proc. of the 8th Intl. Symp. on Environmental Degradation of Materials in Nuclear Power Systems-Water Reactors, S. M. Bruemmer, ed., American Nuclear Society, La Grange Park, IL, pp. 357-365, 1997.

125. Johnson, L. G., "The Median Ranks of Sample Values in Their Population with an Application to Certain Fatigue Studies," Ind. Math, 2, pp. 1–9, 1951.

126. Lipson, C., and N. J. Sheth, "Statistical Design and Analysis of Engineering Experiments," McGraw Hill, New York, 1973.